

Plume-driven subduction termination in 3-D mantle convection models

Erin Heilman¹ and Thorsten Wolfgang Becker¹

¹University of Texas at Austin

March 05, 2024

Abstract

The effect of mantle plumes is secondary to that of subducting slabs for modern plate tectonics, e.g. when considering plate driving forces. However, the impact of plumes on tectonics and planetary surface evolution may nonetheless have been significant. We use numerical mantle convection models in a 3-D spherical chunk geometry with damage rheology to study some of the potential dynamics of plume-slab interactions. Substantiating our earlier work which was restricted to 2-D geometries, we observe a range of interesting plume dynamics, including plume-driven subduction terminations, even though the new models allow for more realistic flow. We explore such plume-slab interactions, including in terms of their geometry, frequency, and the overall effect of plumes on surface dynamics as a function of the fraction of internal to bottom heating. Some versions of such plume-slab interplay may be relevant for geologic events, e.g. for the inferred ~183 Ma Karoo large igneous province formation and associated slab disruption. More recent examples may include the impingement of the Afar plume underneath Africa leading to disruption of the Hellenic slab, and the current complex structure imaged for the subduction of the Nazca plate under South America. Our results imply that plumes may play a significant role not just in kick-starting plate tectonics, but also in major modifications of slab-driven plate motions, including for the present-day mantle.

1 **Plume-driven subduction termination in 3-D mantle** 2 **convection models**

3 **Erin Heilman^{1,2} and Thorsten W. Becker^{1,2,3}**

4 ¹Institute for Geophysics, Jackson School of Geosciences, The University of Texas at Austin, Austin TX,
5 USA

6 ²Department of Earth and Planetary Sciences, Jackson School of Geosciences, The University of Texas at
7 Austin, Austin TX, USA

8 ³Oden Institute for Computational Sciences, The University of Texas at Austin, Austin TX, USA

9 **Key Points:**

- 10 • mantle plumes can terminate subduction in 3-D, damage rheology convection
- 11 • plumes can modulate subducting slabs and plate tectonic regimes
- 12 • plume-slab interactions are plausible contributions to the Karoo-Gondwana event

Corresponding author: Erin Heilman, eheilman@lanl.gov

Abstract

The effect of mantle plumes is secondary to that of subducting slabs for modern plate tectonics, e.g. when considering plate driving forces. However, the impact of plumes on tectonics and planetary surface evolution may nonetheless have been significant. We use numerical mantle convection models in a 3-D spherical chunk geometry with damage rheology to study some of the potential dynamics of plume-slab interactions. Substantiating our earlier work which was restricted to 2-D geometries, we observe a range of interesting plume dynamics, including plume-driven subduction terminations, even though the new models allow for more realistic flow. We explore such plume-slab interactions, including in terms of their geometry, frequency, and the overall effect of plumes on surface dynamics as a function of the fraction of internal to bottom heating. Some versions of such plume-slab interplay may be relevant for geologic events, e.g. for the inferred ~ 183 Ma Karoo large igneous province formation and associated slab disruption. More recent examples may include the impingement of the Afar plume underneath Africa leading to disruption of the Hellenic slab, and the current complex structure imaged for the subduction of the Nazca plate under South America. Our results imply that plumes may play a significant role not just in kick-starting plate tectonics, but also in major modifications of slab-driven plate motions, including for the present-day mantle.

Plain Language Summary

Subduction of cold, strong lithospheric slabs is the main plate driving force within mantle convection. However, hot upwellings, mantle plumes, may have a greater role in modulating plate motions and slab trajectories than previously thought. We use 3-D numerical convection models that account for the weakening of rocks due to the accumulation of deformation to understand the effect that mantle plumes can have on subduction zones. We show that plumes can terminate subduction in a range of circumstances. We also test the effect of the amount of internal heating compared to heat from the core which is the major convective control on the importance of plumes. We discuss cases where these plume-slab terminations may have occurred on Earth, in the geological past, and for the present day through plate reconstructions and consideration of seismic tomography.

1 Introduction

Subduction of the cold, lithospheric boundary layer is the main driving force of plate tectonics through slab pull due to temperature-dependent viscosity and the dominance of internal heating in mantle convection. However, there is also feedback between subducting slabs and mantle plumes as long as there is some degree of bottom heating. While instabilities of the bottom thermal boundary layer can form plumes anywhere, a perturbation, for instance due to a subducting slab, will affect the timing and location for the formation of mantle plumes (e.g. Tan et al., 2002; Dannberg & Gassmüller, 2018; Arnould et al., 2020). This phenomenon suggests a possible feedback, or “talk-back”, between plumes and slabs. Hence, when mantle plumes reach the top thermal boundary layer, i.e. the lithosphere, they too can perturb the cold thermal boundary layer, e.g. creating hotspot volcanics and large igneous provinces (LIPs), contributing to rifting and supercontinental breakup, subduction initiation, and contributing to a low viscosity asthenosphere (e.g. Koppers et al., 2021). When plumes reach the lithosphere at a subduction zone they can interact with slabs by temporarily speeding up plates (van Hinsbergen et al., 2011; Puskok & Stegman, 2020), affecting trench motion and convergence rates (Betts et al., 2012; Mériaux et al., 2015), being deflected by slabs (Druken et al., 2014; Kincaid et al., 2013), or disrupting slabs (Liu & Stegman, 2012; Heilman & Becker, 2022).

Such plume-slab disruption has been less well explored because one may expect a strong, thick slab to survive any plume-induced deformation. As a consequence, when discussing plume-slab interactions, most think of plumes as a possible driver to initiate subduction, and plume-affected plate tectonics has been explored in several models. Plumes may kick-start subduction either directly or by means of emplacing surface density contrasts (Ueda et al., 2008; Rey et al., 2014; Gerya et al., 2015; Baes et al., 2020), and plume induced modification of plate speeds may lead to far field forces for subduction initiation (van Hinsbergen et al., 2021).

However, if strain-dependent damage rheologies, e.g. akin to those explored by Gerya et al. (2021) implemented in simplified form following Fuchs and Becker (2021), are accounted for, plumes do in fact appear capable of terminating subduction as well (Heilman & Becker, 2022). This process can also be associated with an interesting feedback loop of subducting slabs initiating mantle plumes at the core–mantle boundary, plumes terminating subduction close to the surface after their ascent through the mantle, and the

75 broken-off slabs descending through the mantle to possibly begin the process again. While
76 this would, of course, be just one aspect of the time-dependent convection system includ-
77 ing possibly episodic or irregular plate tectonic motions, it is one interaction loop that
78 leaves possibly diagnostic traces in rock record. For example, Fletcher and Wyman (2015)
79 identified that in the past 60 Ma, 18 plumes have been within 1000 km of subduction
80 zones, which points to plume-slab interactions, and potential terminations, as a relevant
81 process to consider for the evolution of the plate tectonic system. Heilman and Becker
82 (2022) explored the effects of internal heating, and thickness, or average temperature/age,
83 of slabs as controlling factors for the likelihood of plumes terminating slabs and mod-
84 ifying the overall tectonic regime, such as a transition from plate-tectonics to stagnant
85 lid. However, our earlier work was limited to 2-D, and one may rightly ask if such a re-
86 striction of flow is a precondition for plume-slab termination.

87 Investigating the nature of plume-slab termination in 3-D is both more realistic and
88 more challenging. For the present-day mantle, we appear to mainly see plume-slab in-
89 teractions where plumes are taking advantage of existing slab windows or tears, formed
90 by plate reorganizations or local slab dynamics (Obrebski et al., 2010; Betts et al., 2012;
91 Portner et al., 2017, 2020). Previously, Betts et al. (2012) showed based on 3-D mod-
92 eling that a plume could modulate subduction in the case of trench rollback causing a
93 subducting slab to move over a plume head. In this instance, a slab window was formed
94 and subduction continued once the slab rolled completely over the plume head.

95 Investigations of suggested recent plume advance include the case of Canary to-
96 ward the Alboran slab underneath the Atlas mountains (Duggen et al., 2009; Sun et al.,
97 2014; Mériaux et al., 2015) and Afar toward Anatolia and the Hellenic subduction zone
98 (Ershov & Nikishin, 2004; Faccenna et al., 2013; Hua et al., 2023). Present-day settings
99 include the Yellowstone/Farallon case (Obrebski et al., 2010; Liu & Stegman, 2012) and
100 the South American Juan de Fuca plume-slab window (Portner et al., 2017, 2020). These
101 studies point to the lithosphere, e.g. in terms of slab tears or windows during trench roll-
102 back, or delamination, being the dominant control, and mantle plumes being secondary
103 to lithosphere dynamics. Plume-slab termination in 3-D will depend on the lateral ex-
104 tents necessary for the interaction to cover, and thermo-mechanical heterogeneity of the
105 mantle and crust. In particular, subduction termination can potentially become easier
106 when damage rheologies or other tectonic inheritance leads to weakening of slabs, includ-

107 ing by segmentation and tears (van Hunen & van den Berg, 2008; Betts et al., 2012; Gerya
108 et al., 2021).

109 Here, we model 3-D, mantle convection in a spherical “chunk” geometry with dam-
110 age rheology and a mixed heating regime similar to Earth’s convective vigor. We explore
111 how damage rheology affects plume-slab interactions and show that plume-induced slab
112 termination is indeed possible in 3-D. We discuss possible instances where this may have
113 happened from the geologic record and present-day seismic tomography to relate our nu-
114 merical models to the Earth.

115 2 Model Setup

116 To model mantle convection as a fluid convection problem in the infinite Prandtl
117 number and incompressible, Boussinesq approximation, we can express conservation of
118 momentum and mass as

$$119 \quad -\nabla \cdot [2\eta\varepsilon(\mathbf{u})] + \nabla p = \rho\mathbf{g} = \rho_0\alpha(T - T_{ref}) \quad (1)$$

$$120 \quad \nabla \cdot \mathbf{u} = 0, \quad (2)$$

122 and conservation of energy without shear heating as

$$123 \quad \rho C_p \left(\frac{\partial T}{\partial t} + \mathbf{u} \cdot \nabla T \right) - \nabla \cdot k \nabla T = \rho H, \quad (3)$$

124 while allowing for advection of a compositional or general tracer field c

$$125 \quad \frac{\partial c}{\partial t} + \mathbf{u} \cdot \nabla c = 0. \quad (4)$$

126 Here, ε is the strain-rate tensor, \mathbf{u} velocity, p pressure, g gravity, T temperature, ρ den-
127 sity, with a reference of ρ_0 at T_{ref} , C_p specific heat capacity, k thermal conductivity, H
128 the internal heat production, η viscosity, α thermal expansivity, and c composition. Eqs. (1)
129 and (2) capture laminar Stokes flow, driven by thermal body forces, and eq. (3) describes
130 the temperature field that is diffused and advected with the flow velocity \mathbf{u} , where the
131 right-hand term is internal heat production. Eq. (4) governs how diffusion-free compo-
132 sitional fields evolve over time; in our models the compositional field tracked is a pas-

133 sive, effective “strain” property used to approximate damage evolution, as in Fuchs and
 134 Becker (2019, 2021), and does not involve additional, e.g., density contributions.

135 To solve eqs. (1-4), we use the open-source, finite element mantle convection code
 136 *ASPECT* (Kronbichler et al., 2012; Heister et al., 2017; Fraters et al., 2019). Our ap-
 137 proach overall follows that of Heilman and Becker (2022), but we employ a Newtonian,
 138 Frank-Kamenetskii linearized temperature-dependent viscosity law (cf. Tackley, 2000a;
 139 Stein & Hansen, 2013) to simplify the model for a 3-D test case. The equation is as fol-
 140 lows,

$$141 \quad \eta(T) = \eta_{ref} \exp \left[\frac{E}{1 + \frac{T}{T_{ref}}} - \frac{E}{2} \right] \quad (5)$$

142 where η_{ref} is a reference viscosity, E is a non-dimensional activation energy, and T_{ref}
 143 is a reference temperature. Added into this viscosity law is a viscosity jump at 660 km
 144 depth, where the η_{ref} is increased by a factor of 30 in the lower mantle, as expected from
 145 geoid modeling and slab sinking rates (e.g. Hager, 1984; Ricard et al., 1993; Steinberger
 146 & Calderwood, 2006).

147 Additionally, we include visco-plasticity and a simplified damage rheology in our
 148 models (e.g. Tackley, 2000b; Ogawa, 2003; Auth et al., 2003; Fuchs & Becker, 2019). *AS-*
 149 *PECT* employs plasticity and a possible strain-weakening for modulating the yield stress
 150 (Glerum et al., 2018). When the viscous stress ($2\eta\dot{\epsilon}_{II}$) exceeds the yield stress the vis-
 151 cosity is rescaled back to an effective yield viscosity (e.g., Moresi & Solomatov, 1998; Enns
 152 et al., 2005).

$$153 \quad \eta_{eff} = \frac{\sigma_y}{2\dot{\epsilon}_{II}}. \quad (6)$$

154 We then use a strain-based damage variable γ to reduce the yield stress from the back-
 155 ground value (e.g. Lavier et al., 2000; Ogawa, 2003). Damage, γ , evolves according to

$$156 \quad \frac{d\gamma}{dt} = \dot{\epsilon}_{II} - \gamma A_d \cdot \exp [E_d (T - T_0)] \quad (7)$$

157 where $\dot{\epsilon}_{II}$ is the second invariant of the strain-rate tensor, A_d is a timescale for strain-
 158 healing, E_d is a non-dimensional activation energy, following temperature- and time-dependent
 159 strain healing (Fuchs & Becker, 2019). Combining plasticity and such a damage rheol-
 160 ogy, which incorporates strain-weakening and strain-healing, can approximate the be-
 161 havior of physical weakening processes like those inferred from grain-size dependent rhe-

Table 1. Model parameters

Parameter	Value
Temperature difference between thermal boundary layers	2373 K
Density ρ	3700 kg/m ³
Thermal expansivity α	$2 \cdot 10^{-5}$ K ⁻¹
Thermal diffusivity κ	10^{-6} m ² /s
Specific heat capacity C	750 J/gK
Internal heating rate H	$5.0 \cdot 10^{-12}$ W/kg
Minimum viscosity η_{min}	10^{18} Pas
Maximum viscosity η_{max}	$2.5 \cdot 10^{24}$ Pas
Non-dimensional activation energy E	29.95
Reference viscosity η_{ref}	$4.5 \cdot 10^{19}$
Reference temperature for viscosity T_{ref}	2500 K
Yield stress for Damage Model	140 MPa
Minimum weakened yield stress for Damage Model	35 MPa
Yield stress for No Damage Model	55 MPa
Non-dimensional strain weakening factor s.w.f.	0.25
Non-dimensional activation energy for strain healing E_d	250
Non-dimensional timescale for strain healing A_d	10^{-7}

162 ologies (Fuchs & Becker, 2021), which is one of the suggested mechanisms for strain lo-
163 calization (e.g. Landuyt & Bercovici, 2009; Bercovici & Ricard, 2016). The strain-weakening
164 factor (Table 1) is set to reduce the yield stress linearly by 75%, i.e. from 140 to 35 MPa,
165 with parameters based on our earlier work. This accumulation/healing formulation al-
166 lows damage to persist and be advected in cold lithosphere while damage in the man-
167 tle is healed according to a specified rate with temperature (Table 1). We compare a model
168 with damage rheology to a model without to understand the effect of damage on the abil-
169 ity of mantle plumes to terminate subduction.

171 Temperature boundary conditions for our mixed heating convection model are 273 K
172 and 2573 K for the surface and core-mantle boundary, respectively, and the mechani-
173 cal boundary conditions are free slip on all sides. We use a reference internal heating value
174 of $5 \cdot 10^{-12}$ W/kg (Table 1) and compare the effect of different internal heating produc-
175 tion rates in subsequent models. The Earth's ratio of internal to bottom heating is in-
176 completely constrained and expected to be time-variable over planetary history because
177 of the decay of radiogenic material. We expect the balance of bottom to internal heat-
178 ing to control the relative importance of mantle plumes from a general understanding
179 of mantle convection (e.g. Davies, 1986; Zhong, 2006; Leng & Zhong, 2008; Foley & Becker,
180 2009) and our earlier, 2-D tests (Heilman & Becker, 2022).

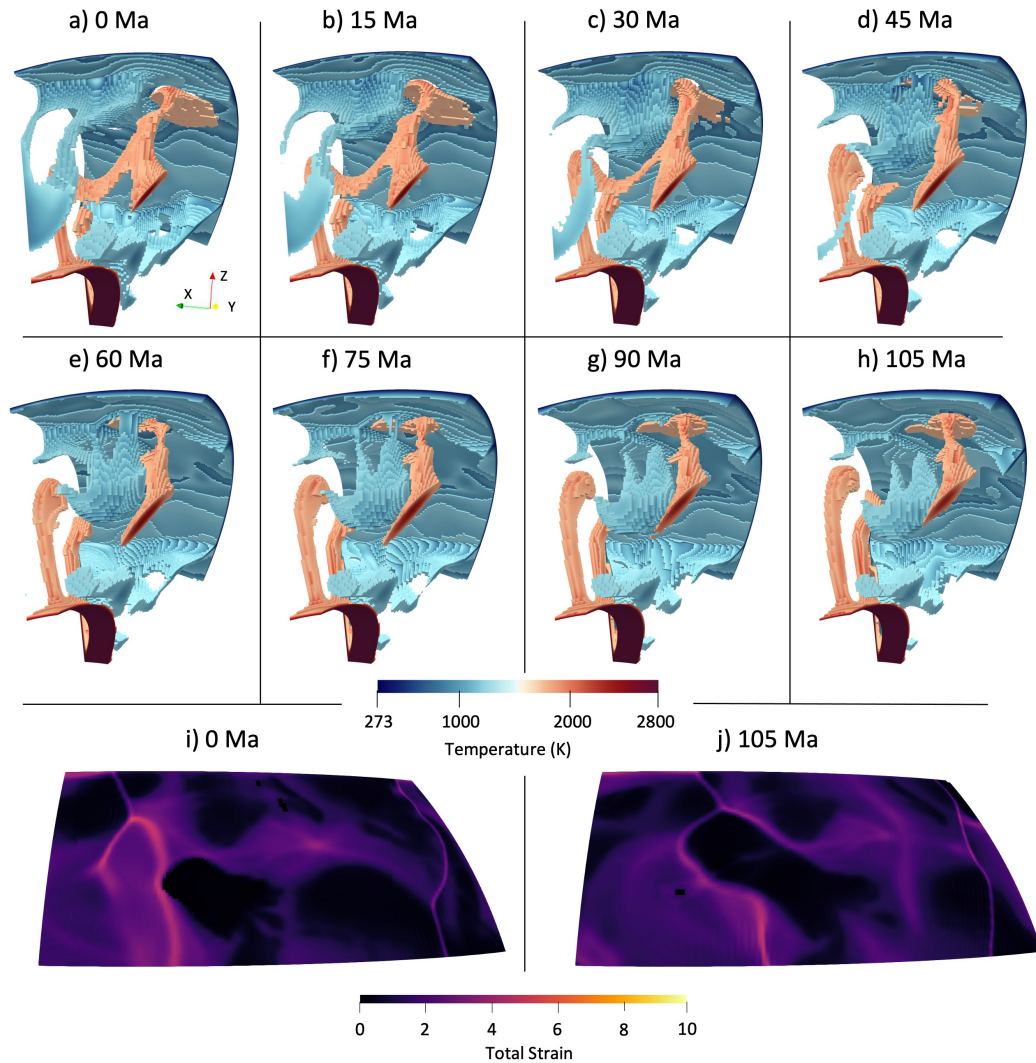
181 We compare our reference model with a non-damage rheology case, which requires
 182 a lower yield stress to roughly match the convective vigor of the models with damage
 183 (cf. Fuchs & Becker, 2022). The effective Rayleigh number of our reference computation
 184 is $\sim 3.5 \cdot 10^6$. Bulk metrics such as surface heat flow are in Earth-like ranges (sec. 3.3),
 185 with surface velocities ~ 3 times lower than for present-day plate speeds. We thus ex-
 186 pect the dimensionalized model times to broadly correspond to actual time for our ref-
 187 erence models. However, to make models with different parameters and hence convec-
 188 tive vigor overall comparable, e.g., in terms of frequency of tectonic events, we also re-
 189 port times in units of overturn time, i.e. the typical time taken for a density anomaly
 190 to traverse the mantle and back. For the Earth, those can be converted by multiplying
 191 with relevant timescales, ~ 300 Myr for ~ 2 cm/yr average vertical motions.

192 **3 Results**

199 **3.1 Damage Rheology Model**

200 We first explore a model with the damage rheology and a yield stress of 140 MPa
 201 (Figure 1) building on the work by Heilman and Becker (2022). Including damage rhe-
 202 ology in a convection model leads to potential localization of deformation, formation of
 203 persistent weak zones (e.g. Auth et al., 2003; Landuyt et al., 2008), as well as possibly
 204 an overall drop in bulk lithospheric strength, e.g. if damage reduces the yield stress (cf.
 205 Foley & Bercovici, 2014; Fuchs & Becker, 2019, 2022). In our models, the damage rhe-
 206 ology weakens the subducting slabs and allows the weakness to persist because the slabs
 207 are cold. When mantle plumes strike the lithosphere, the damage is reduced as the plumes
 208 introduce heat. This can lead to the healing effect to take over, reducing the associated
 209 inherited weak zones on the surface. This does not mean that plumes make the litho-
 210 sphere strong in our models, they still tend to decrease the viscosity of the lithosphere
 211 that they underplate, and generally lead to some mode of extension on the surface.

212 To visualize the plume-slab interactions and terminations we applied a tempera-
 213 ture threshold for both the mantle plumes and subducting slabs. This thresholding al-
 214 lowed us to visualize features and interactions easily in 3-D. Figure 1a-h shows the tem-
 215 perature thresholding on the left for a plume-slab termination event. The total accumu-
 216 lated strain on the surface in Figure 1i-j shows the influence of the hot plume on the sub-
 217 duction zone in terms of damage. As the plume terminates subduction, the damage that



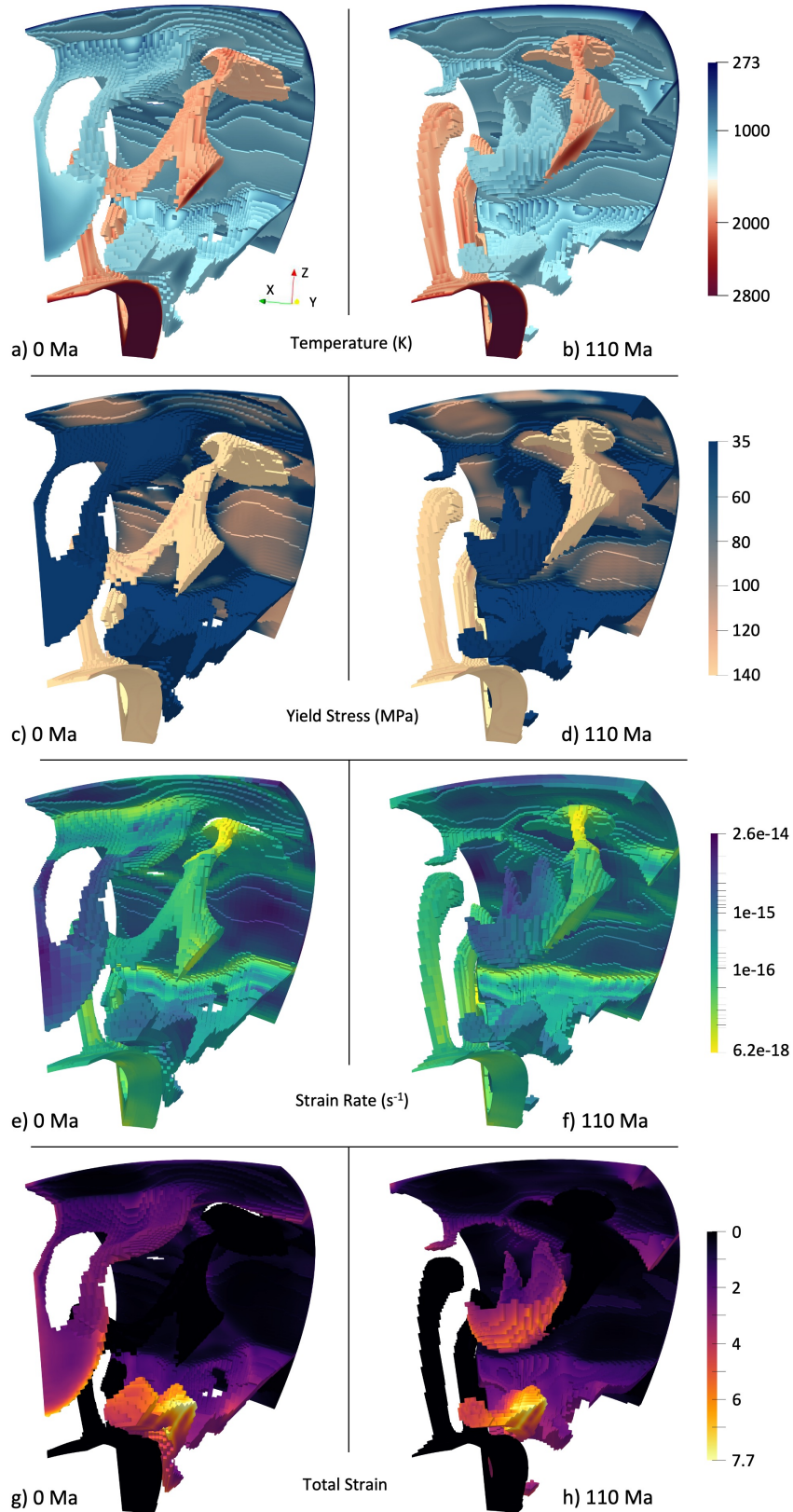
193 **Figure 1.** Example of a rising mantle plume terminating an subduction zone in 3-D for our
 194 reference model with damage. a-h show temperature thresholds of plumes (~ 1750 - 2773 K, red
 195 colors) and slabs (273 - ~ 1250 K, blue) over several timesteps showing a plume-slab interactions.
 196 Plots i-j show the damage, expressed as effective “strain”, at the surface at the first and last
 197 timestep. When the plume strikes the surface, it resets the damage and it influences the subduc-
 198 tion zone to bend around it.

218 was accumulated in the subduction zone in the lithosphere (Figure 1i) deflects around
219 where the plume head strikes the lithosphere (Figure 1j), because the plume head intro-
220 duces heat to the lithosphere which then increases the amount of strain healed above the
221 plume. This configuration of damage remains frozen in the lithosphere and is advected
222 along the surface until a new subduction zone is initiated from the damaged arc (cf. Fo-
223 ley & Bercovici, 2014; Fuchs & Becker, 2019; Heilman & Becker, 2022).

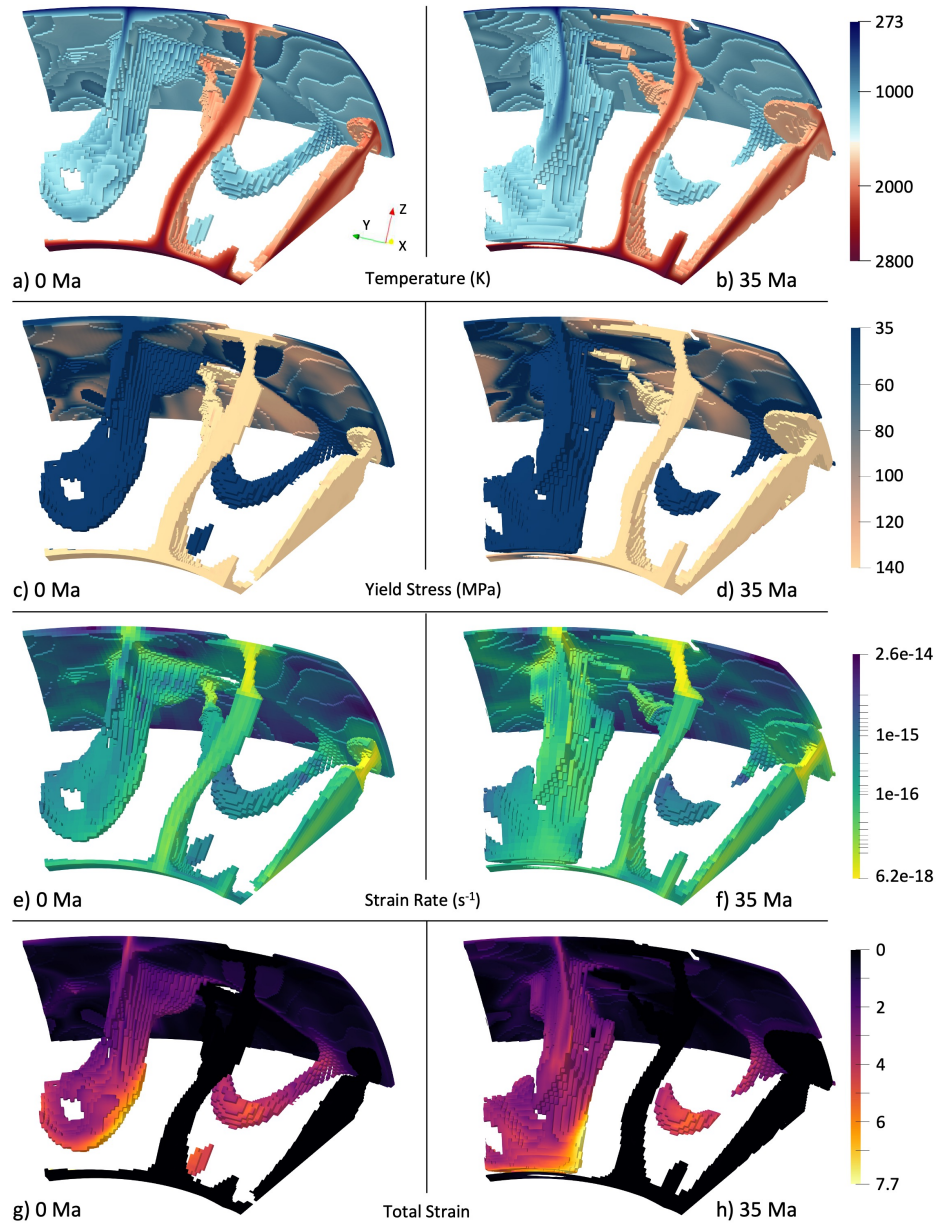
224 The reference model ran for a total of 3 model overturns, beginning from an ini-
225 tial steady state model run. During the qualifying model run time of 3 overturns, we ob-
226 serve 7 instances of plume-slab termination, i.e. an average of 2.3 terminations every over-
227 turn. In these models, termination of subduction is quantified through the temperature
228 thresholding when no part of the subducting slab is connected to the trench of the sub-
229 duction zone. These termination events do not tend to overlap in time, however we do
230 observe an instance when two terminations are present at the same time. Terminations
231 are clustered in time, with periods of quiescence, similar to what was observed and an-
232 alyzed by Heilman and Becker (2022).

233 Six of the seven termination events occurred with a single plume impinging on a
234 subduction zone causing the termination. The six events do vary in where the plume in-
235 teracts with the slab along its lateral extent. If the plume strikes the center of the sub-
236 ducting slab, the termination tends to develop by creating a slab window that then ex-
237 tends along the length of the slab until it is fully terminated (as in Figure 1). If the plume
238 head interacts with the slab closer to the subducting slabs lateral extent, then the ter-
239 mination has an unzipping effect as the slab begins detaching at the plume head and con-
240 tinues along the length of the slab. The last termination was caused by two plumes on
241 both sides of the subduction zone that pinched out the subducting slab to shut off sub-
242 duction.

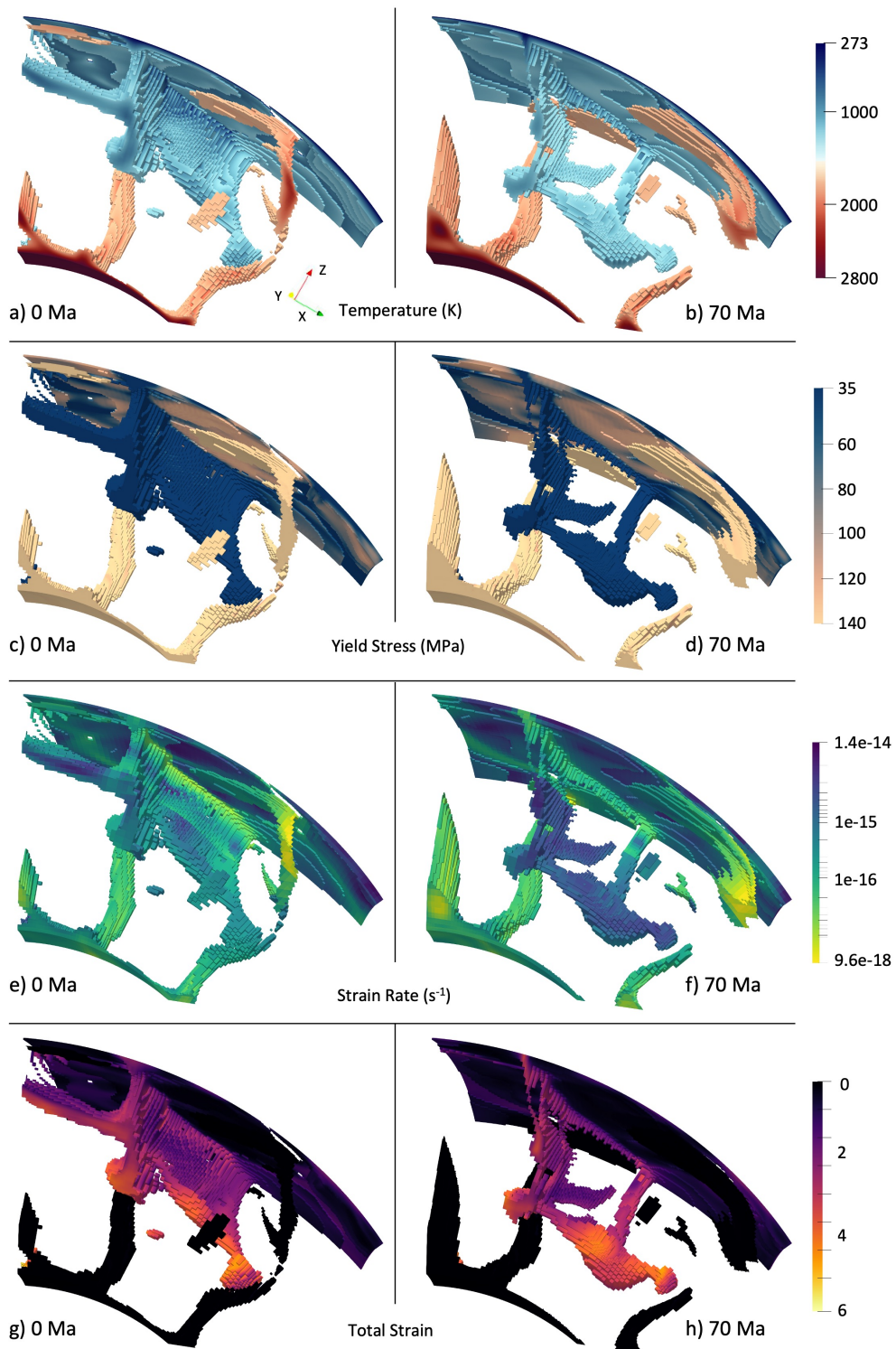
252 Figures 2, 3, and 4 show these styles of termination in temperature, yield stress,
253 strain rate, and total strain (accumulated damage) before and after termination, where
254 termination is inferred from the visualization as the time when the slab is fully detached.
255 We observe in these terminations that the subducting slab is strongly weakened during
256 subduction, while the mantle plume is not further weakened by damage or plasticity, due
257 to its inherent higher temperature (cf. Fuchs & Becker, 2019). Both the mantle plume
258 and the subducting slab, in the area of the most bending in the slab, have high strain



243 **Figure 2.** Temperature, yield stress, strain rate, and accumulated strain (damage) before (a,
 244 c, e, g) and after termination (b, d, f, h) for a typical termination (same termination as Figure 1)
 245 where a plume impinges on a subducting slab and shuts off subduction.



246 **Figure 3.** Temperature, yield stress, strain rate, and accumulated strain (damage) before (a,
 247 c, e, g) and after termination (b, d, f, h) for a termination where a plume impinges on the edge of
 248 a subducting slab and shuts off subduction by unzipping along the slab's length.



249 **Figure 4.** Temperature, yield stress, strain rate, and accumulated strain (damage) before (a,
 250 c, e, g) and after termination (b, d, f, h) for a double-sided termination where two plumes pinch
 251 out a subducting slab to shut off subduction.

259 rates that lessen after termination has occurred. In the case of damage, the subducting
 260 slabs have a moderate (~ 2 -5) amount of accumulated damage. This is a result of the weak-
 261 ening and slow healing in the cool slab, as opposed to the hot mantle plumes that have
 262 no accumulated damage. After termination occurs, the damage persists in the terminated
 263 slab as it sinks in the mantle, until the slab is heated enough that the damage is healed
 264 (cf. Fuchs & Becker, 2019).

265 However, as may be expected, and explored more fully in 2-D (Heilman & Becker,
 266 2022), not every plume-slab interaction ends in a termination. We find at least five in-
 267 stances where a plume interacts with a subducting slab without causing a complete ter-
 268 mination, i.e. a roughly 60% chance of plumes shutting down subduction if they get close
 269 to slabs, for our chosen parameter values. Some of these plume-slab interactions result
 270 in no change to the subducting slab morphology from the plume. While in some cases,
 271 the plume creates a slab window in the subducting slab but subduction is able to con-
 272 tinue normally, as has been suggested for modern settings based on seismic tomography.

273 **3.2 Non-Damage Rheology Model**

274 We include a model without the damage rheology to compare to the plume-slab
 275 interactions we observe in the damage model. In this non-damage model, the background
 276 yield stress has to be lowered to 55 MPa from 140 MPa to achieve the same convective
 277 vigor and maintain a mobile convective regime (comparable Rayleigh number of $\sim 3.8 \cdot 10^6$).
 278 Both of the used yield stress values are required to achieve plate-like motions with a mo-
 279 bile lid in our models, however, the values are much smaller than what would be expected
 280 from rock mechanics. This is a typical finding for visco-plastic, plate-like convection mod-
 281 els (e.g. Moresi & Solomatov, 1998; van Heck & Tackley, 2008; Foley & Becker, 2009),
 282 and might indicate some additional weakening mechanism, such as hydration. However,
 283 our point here is not about the absolute values, but we merely provide an attempt to
 284 compare damage and no-damage cases at similar convective vigor and tectonic style.

285 Our non-damage model has a total run time of ~ 6 overturns, and this model showed
 286 only one example of plume-slab termination. In this termination, a plume first formed
 287 a slab window in a subducting slab, which then caused a slab tear on either side of the
 288 slab window, and lead to the eventual termination of the subduction zone. There were
 289 four other instances where a mantle plume caused the formation of a slab window that

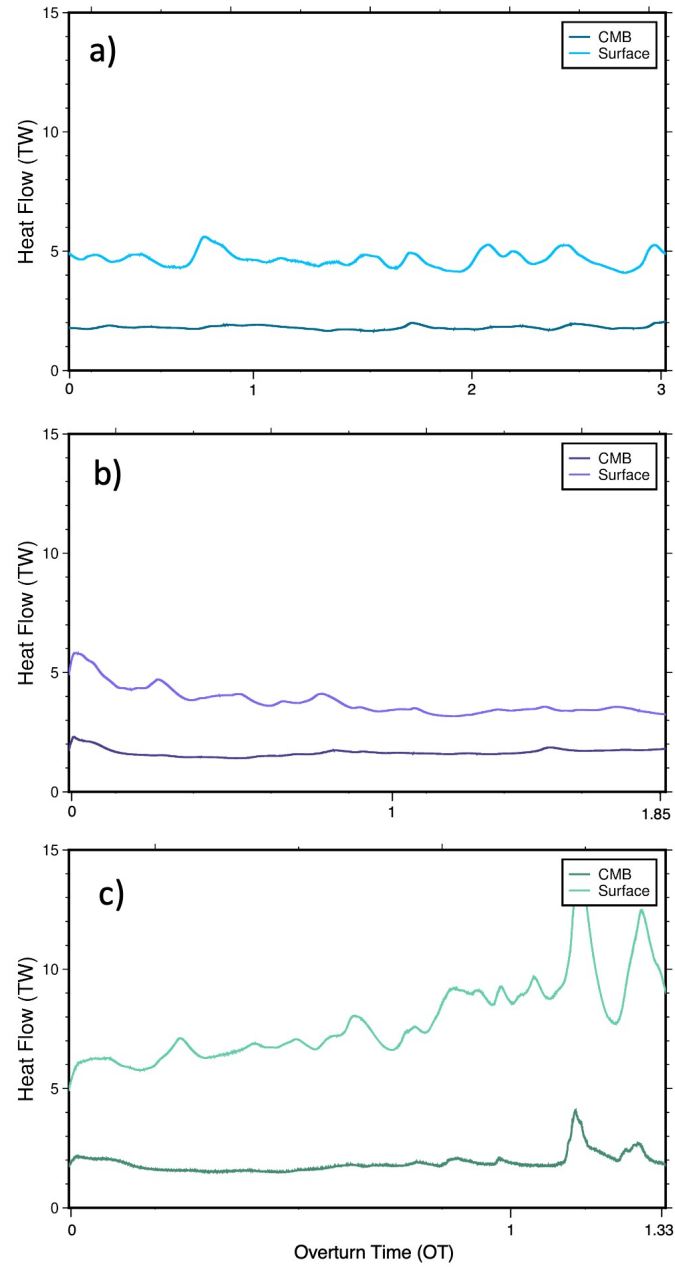
290 did not result in an immediate termination of subduction. In this non-damage rheology
 291 case, the yield stress in the subducting slab can be higher than that in the damage rhe-
 292 ology case due to the lack of weakening. This higher slab yield stress is likely why we
 293 see more formations of slab windows than full plume-slab terminations in our non-damage
 294 model.

295 **3.3 Ratios of Internal Heating**

296 We expect the amount of internal heating to affect the importance of plumes, which
 297 are trivially absent if there is no bottom heating, and whose effect will be maximal for
 298 pure bottom heating. To compare our reference damage rheology results, two other mod-
 299 els were run with a lower ($5 \cdot 10^{-13}$ W/kg) and a higher ($2 \cdot 10^{-11}$ W/kg) amount of
 300 internal heat production, i.e. 0.1 and 4 times the heat production of the initial damage
 301 rheology model. The heat flow time series for the three models are shown in Figure 5.
 302 The average heat flow for the reference model (Figure 5a) is 1.81 TW for the core-mantle
 303 boundary (CMB) and 4.69 TW for the surface. The relative contribution of 61.5% from
 304 internal heating for the reference model is in the ballpark of estimates for the Earth's
 305 mantle (Leng & Zhong, 2008; Lay et al., 2008; Jaupart et al., 2015), which are, however,
 306 uncertain. The average heat flow for the lower heating model (Figure 5b) is 1.67 TW
 307 out of the CMB and 3.77 TW out of the surface, for 55% contribution from internal heat-
 308 ing. The average heat flow for the higher heating model (Figure 5c) is 1.76 TW out of
 309 the CMB and 7.27 TW out of the surface, for 75% contribution from internal heating.

310 Considering absolute values, our 3-D spherical chunk is roughly 15% of the surface
 311 area of the Earth. Scaling the heat flow out of the surface of the model to Earth would
 312 be roughly 31.3 TW for the reference model, and 25.1 TW and 48.5 TW for the lower
 313 and higher heating model, respectively. These values are comparable to estimates for the
 314 convective heat flow of the mantle, ~ 38 TW (Jaupart et al., 2015). This implies that while
 315 our focus here is, of course, mainly to explore the general controls on plume dynamics,
 316 and we did not account for secular cooling, the overall convective vigor of the models may
 317 be comparable to the mantle.

320 While having only changed the internal heat production, complexities arise because
 321 different average viscosities result via the temperature-dependent creep laws used. This
 322 means that these models have different Rayleigh numbers, or convective vigor, with es-



318 **Figure 5.** Heat flow out of the CMB and surface are plotted over overturn times for three
 319 models. a) Damage Model. b) Lower Internal Heating Model. c) Higher Internal Heating Model.

323 timates for the Rayleigh numbers $4.65 \cdot 10^5$, $9.95 \cdot 10^6$, and $7.16 \cdot 10^7$ for the lower, ref-
324 erence, and higher heating cases, respectively. This changing convective vigor does have
325 an effect on the planform of convection. However, these models all remain predominantly
326 mobile and in a plate tectonic-like convection regime, meaning they should be broadly
327 comparable in terms of their dynamics, including plume-slab interactions.

328 The model with a lower proportion of heating ran for a total of 1.85 overturns from
329 an initial steady state model. This model showed eleven plume-slab terminations, i.e.
330 roughly 5 per overturn. These terminations follow the same trend as in the reference model,
331 where the subducting slab is fully weakened before the termination, strain rate is high
332 in both the slab and plume and lessens after termination, and the subducting slab is dam-
333 aged prior to termination. We also see in this model a non-termination event creating
334 a slab window in the subducting slab and subduction continues. Specifics of these in-
335 teractions and the detailed numbers of terminations per a given typical model time are,
336 of course, subject to stochastic fluctuations.

337 The model with a higher proportion of heating had a total run time of 1.33 over-
338 turns after starting from an initial steady state model. This model showed two plume-
339 slab terminations, i.e. ~ 1.5 terminations per one overturn. This model had hotter av-
340 erage mantle temperatures (2034 K compared to the reference model 1518 K) and there-
341 fore hotter subducting slab temperatures due to the increased proportion of internal heat-
342 ing. It was more difficult to identify instances when plumes were actively shutting off
343 subduction as the hotter mantle led to the subducting slabs warming quickly and de-
344 taching even without plume influence. The model becomes unstable towards the end of
345 its run time and moves into an episodic regime (as seen in Figure 5c) and may be more
346 relevant for ealy Earth rather than, say, Cenozoic mantle convection (e.g. van Hunen &
347 van den Berg, 2008).

348 Given variations in the relative importance of bottom and internal heating, we thus
349 find the expected effect on the rate of plume-slab terminations per overturns. All mod-
350 els show plume-slab terminations and interactions, but for the lower internal heating model
351 the frequency of plume-termination events was almost double the reference model. The
352 opposite is true for the higher internal heating model with fewer plume driven subduc-
353 tion terminations, substantiating the 2-D results of Heilman and Becker (2022). We also
354 ran two other models with intermediate heat production of $8 \cdot 10^{-12}$ W/kg and $1 \cdot 10^{-11}$ W/kg

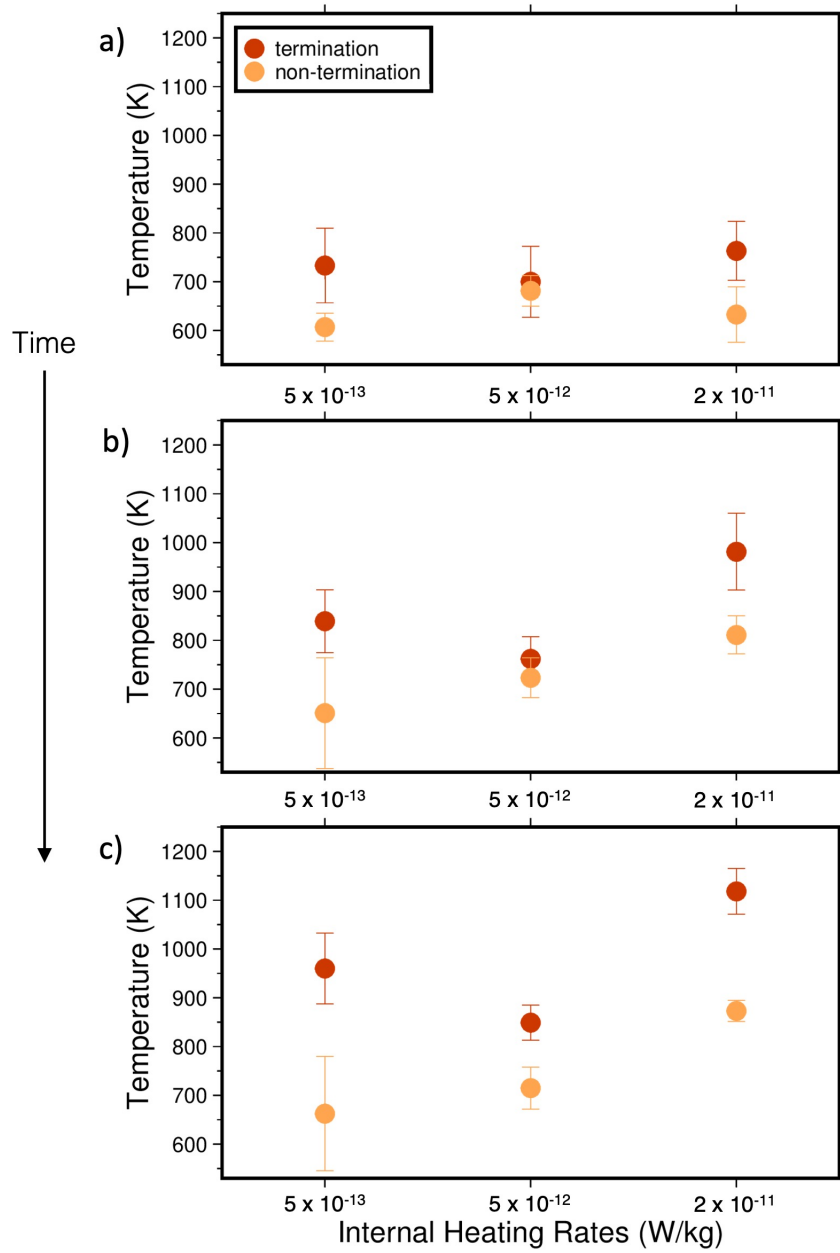
355 for validation and the termination numbers were in between the higher heat model and
356 the reference model.

357 Due to the additional degrees of freedom provided by 3-D flow compared to the anal-
358 ysis of Heilman and Becker (2022), and the highly time-dependent nature of the convec-
359 tive system, further, systematic analysis of controlling factors beyond the overall effect
360 of internal heating has to be somewhat limited. We measured internal slab temperature
361 for both terminating and non-terminating plume-slab interactions by sampling temper-
362 atures from the subducting slab for a period of 60 Ma (well within the overall termina-
363 tion and interaction times). The temperatures were collected over a 50 km section of the
364 subduction zone where the plume was actively interacting with it, at a spacing of 10 km
365 intervals. These data were averaged over the length (50 km) and the standard deviation
366 was taken to show the variability of temperature within the slab. In general, we find that
367 the non-terminating interactions are typically happening for slabs that are colder and
368 hence thicker, as expected (Heilman & Becker, 2022).

372 We plot slab temperatures for terminations and non-terminations as a function of
373 internal heating in Figure 6. As the average mantle temperature increases, plumes con-
374 tribute less to the convective dynamics, so there are less terminations overall. For these
375 models, the respective average mantle temperatures are 1278, 1518, and 2034 K. The age
376 of thickness of the subducting slab as reflected in our temperature estimates during non-
377 terminations follows this trend as well, shown most clearly in Figure 6c where the non-
378 termination temperatures increase with the proportion of internal heating.

379 **4 Discussion**

380 Our models show that plume-driven subduction terminations occur in 3-D spher-
381 ical geometry convection models, substantiating the suggestion of Heilman and Becker
382 (2022). This implies that plume-induced subduction termination may indeed happen on
383 Earth, if convective vigor and actual rock rheology are similar to those represented by
384 our model. A prerequisite for termination is that the slab can be weakened, as is the case
385 for our damage rheology model. While slab pull forces can be supported for plate-like
386 motions even in the presence of weakening (cf. Gerya et al., 2021), the accumulated dam-
387 age makes it easier for the mantle plume to cut through, or pinch out, the subducting
388 slab (Figures 2, 3, and 4). While it is perhaps becoming more broadly accepted that the



369 **Figure 6.** Subducting slab temperatures for terminations and non-terminations for each ratio
 370 of internal heating. Plots a), b), and c) increase in 20 Ma time increments showing the trend in
 371 slab temperature over time for each internal heating ratio.

389 lithosphere is significantly weakened in the trench region where the plate is bending, our
390 rheological choices may, of course, lead to slabs that are weaker than in the Earth's man-
391 tle. However, since slab segmentation is a widely inferred process (e.g. Tan et al., 2002;
392 Liu & Stegman, 2012), we would expect plume-slab terminations for stronger slabs to
393 be perhaps less frequent on Earth than in our models, rather than being completely ab-
394 sent.

395 Besides rheology, the other control on the importance of plume-slab interactions
396 is the degree of bottom to internal heating. Our results for a higher to lower rate of in-
397 ternal heating (sec. 3.3 and Figure 6) could be interpreted as being indicative of the evo-
398 lution of mantle dynamics from the early Earth to present-day. As the internal heating
399 of the mantle has decreased by a factor of ~ 4 over time with an effective decay timescale
400 of ~ 3 Ga (e.g. Jaupart et al., 2015) due to the half life of radiogenic elements, there will
401 be a greater effect of mantle plumes during the more recent periods of plate tectonics,
402 including relatively more frequent plume-induced subduction terminations. Such effects
403 due to active upwellings may add to the possible contributions of accumulating damage
404 and persistent sutures in the lithosphere to make plate tectonics more time-dependent
405 toward the present, even though the overall convective vigor may decrease with progres-
406 sive cooling (Foley & Bercovici, 2014; Fuchs & Becker, 2022).

407 As our models are freely convecting, rather than being tailored to specific tectonic
408 scenarios, we can only make observations about what sorts of subduction zones get ter-
409 minated and what the typical geometry and dynamics of those cases are. The main sce-
410 narios we observe are a plume head impinging either in front or behind the subducting
411 slab to cause termination (Figures 2 and 3) and plumes on either side of a subducting
412 slab pinching out a subduction zone leading to termination (Figure 4). The first exam-
413 ple is most common in the model, occurring $\sim 85\%$ of the time in the reference, damage-
414 rheology model, and it is the only mode in the non-damage rheology, lower internal heat-
415 ing, and higher internal heating cases. Typically, this process begins as a plume initi-
416 ating a slab window in the subducting slab. The plume can then either remain station-
417 ary with the subduction zone and the termination happens in the plume's presence, or
418 the plume may advect or diffuse away from the subducting slab, but the influx of heat
419 from the plume was enough to cause the termination. The second scenario has two plumes
420 pinching out a subduction zone to cause a termination. We see this type of termination

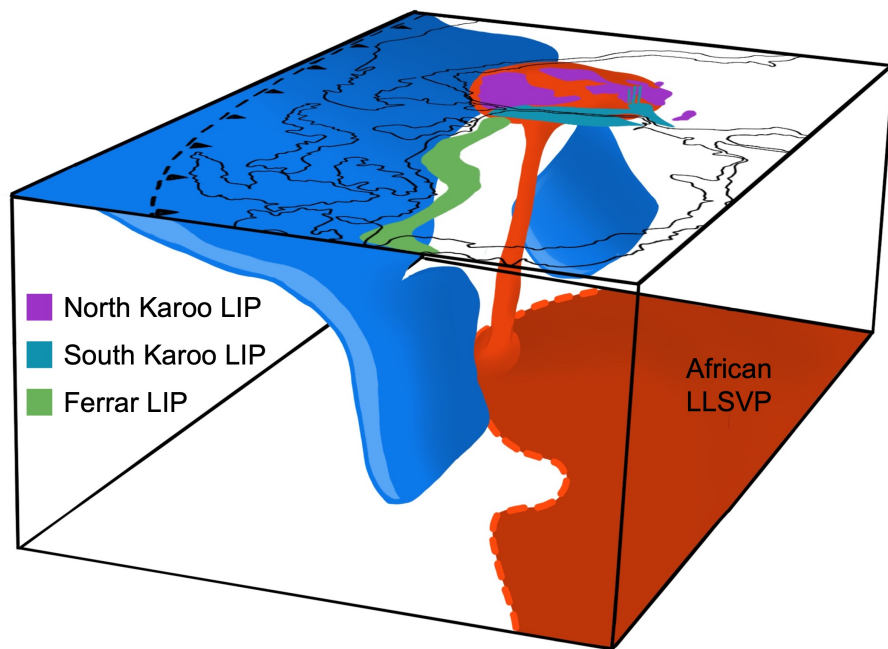
421 less frequently in our models, and this scenario is perhaps also less likely on Earth as it
422 requires plumes on either side of a subduction zone.

423 To discuss disruption frequency of terminations, we must scale back to dimensional
424 Earth time. Thus, we use 300 Myr as an appropriate comparison of overturn time to di-
425 mensional time for Cenozoic mantle convection. The disruption frequency of termina-
426 tions is then one termination every 50 Myr for the lower heating model, every 130 Myr
427 for the reference model, and every 200 Myr for the higher heating model. Additionally,
428 the non-damage model frequency with its one termination would be every 1.8 billion years.
429 This scaling of frequency correlates with the proportion of internal heating of the mod-
430 els, with the most frequent occurring in the model with the highest proportion of bot-
431 tom heating and becoming less frequent with higher proportions of internal heating. This
432 frequency suggests there may be several examples of this plume-slab termination in Earth's
433 history.

434 **4.1 Comparison to past and modern-day tectonic settings**

435 Plume-slab terminations show interesting dynamics in geodynamic models, but there
436 is also some indication of their existence in past and present-day geology. One example
437 during the Jurassic (201-145 Ma) is related to the Karoo-Ferrar LIP eruption in south-
438 western Gondwana. While it is generally agreed that there was a time of flat slab sub-
439 duction previous to the LIP emplacement, there is debate as to how this flat slab sub-
440 duction ended (Dalziel et al., 2000; Luttinen, 2018; Navarrete et al., 2019; Ruhl et al.,
441 2022). Figure 7 shows our interpretation in 3-D of the dynamics of this system, moti-
442 vated by our 3-D model dynamics. If the rising mantle plume was responsible for flat
443 slab subduction (Dalziel et al., 2000), it may have subsequently broke through the slab,
444 reached the lithosphere, and created the Karoo-Ferrar LIP. This scenario can also ex-
445 plain the bilateral geochemical sourcing of the Karoo from both deep mantle sources and
446 subduction-modified upper mantle sources as the plume rises and terminates. The sub-
447 ducting slab could have then unzipped from where the mantle plume broke through, ex-
448 plaining the subduction-influenced upper mantle signature in the Ferrar LIP (Luttinen,
449 2018).

454 A more recent example of plume-slab dynamics is the Arabian-Anatolian-Aegean
455 system (Ershov & Nikishin, 2004; Faccenna et al., 2013; Hua et al., 2023). Subduction

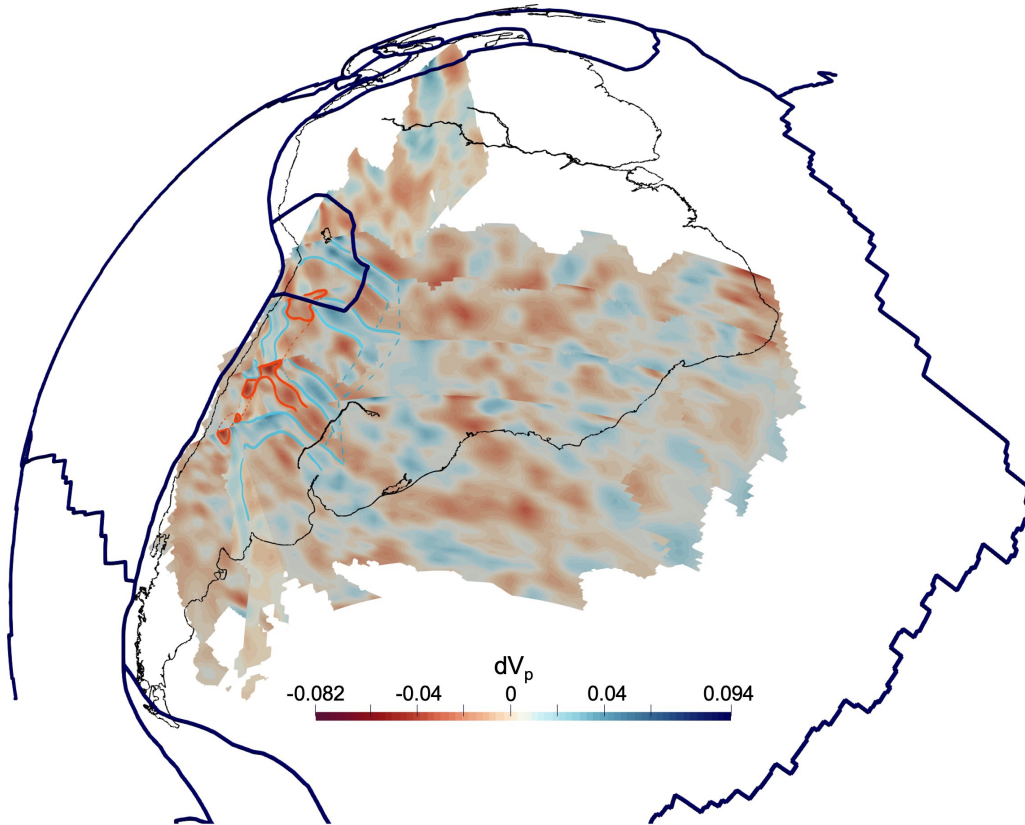


450 **Figure 7.** 3-D reconstruction of southwestern Gondwana during the Jurassic showing on the
451 surface the emplacement of LIPs (Luttinen, 2018). Rendering in the mantle shows projected
452 African LLSVP, mantle plume that cutoff subduction underneath southwestern Gondwana and
453 shows propagation of slab shutoff.

456 in the Mediterranean has been inferred to have been active 30 million years ago as the
457 Afar plume was upwelling under the Arabian plate to the southeast (cf. Faccenna et al.,
458 2013). Volcanic ages and other constraints have been interpreted such that the plume
459 then moved northward toward Anatolia, and that this plume advance was driven or at
460 least assisted by mantle flow, including via a fragmentation of the Mediterranean slab.
461 The formation of a slab gap underneath Anatolia leading to the current Hellenic segment
462 of the trench might have led to asthenospheric suction and contributed to Afar plume
463 advance (Faccenna et al., 2013; Hua et al., 2023). Our results here, and the 2-D mod-
464 els of Heilman and Becker (2022), suggest that the Afar plume may have, in fact, played
465 a more active role in partitioning subduction along the northern margin of Africa.

466 For the modern-day, the Nazca-South American subduction zone may serve as an
467 example for the effect of plumes on slabs. Based on interpretation of seismic tomogra-
468 phy, Portner et al. (2017, 2020) suggested that the Juan de Fuca plume was taking ad-
469 vantage of a previously created slab window. With our model findings, we can specu-
470 late that this interaction is the beginning of a plume-slab termination where a slab win-
471 dow is developed first and a few million years later leads to subduction shutoff. In Fig-
472 ure 8, we interpret the tomography of Portner et al. (2020) for the Nazca slab and man-
473 tle. In this figure the dotted lines are interpretations of the lateral extent of the plume
474 and slab. The mantle plume may have modified and broken through part of the subduct-
475 ing slab. This stage of a plume lying under a subducting slab and creating a slab win-
476 dow is very similar to the beginning stages of several terminations that we observe in
477 our model (i.e. Figure 1). In the future, this interaction may turn into a termination if
478 the slab is sufficiently affected by the presence of the plume.

483 Relevant plume-slab interactions may also be present in other areas for the modern-
484 day, including on the western side of the Pacific where a range of hot anomalies have been
485 imaged in proximity to possibly fragmented slabs (e.g. Obayashi et al., 2009; Tao et al.,
486 2018), and the effects of hot mantle anomalies on subduction have been modeled (e.g.
487 Morishige et al., 2010). Plume-slab interactions in east Asia have been postulated for
488 origin of the Changbaishan volcanic complex, where intraplate volcanism may be driven
489 by a plume disrupting or at least affecting the subducting Pacific plate (Tang et al., 2014).
490 Seismic imaging has been interpreted to show hot material from the deep mantle rising
491 through a gap in the subducting slab (Tang et al., 2014), a type of interaction between
492 plumes and slabs consistent with our model findings.



479 **Figure 8.** Tomography fence diagram of southern South America using dV_p using tomo-
 480 graphic data from Portner et al. (2020). Interpretation of 3D plume-slab interaction structure is
 481 overlain in blue for subducting slab and red for mantle plume. South America is outlined in black
 482 while tectonic plates are outlined in dark blue.

5 Conclusions

We find that plume-induced subduction terminations occurs in 3-D, spherical geometry mantle convection models. Terminations are found throughout our models, but more likely in cases with damage rheology. A single plume can directly shut off subduction by puncturing and cutting off a slab from below, two plumes can pinch out subduction from the side, and a single plume can cause an lateral unzipping of a descending slab. Natural examples where these processes may help explain the thermo-chemical evolution of the continental lithosphere include the Karro-Ferrar LIP, the Afar-Anatolia Aegean system, and present-day settings in the western and eastern Pacific subduction systems. Plume-slab termination frequency is inversely related to the proportion of internal heating, implying that plume-slab interactions may have become more prevalent over planetary evolution. Our models can contribute to a better understanding of the relationship between subducting slabs and rising mantle plumes and the effect and expressions of slab-plume “talk-back” in the evolution of the plate tectonic system.

6 Open Research

ASPECT is an open-source mantle convection code hosted by the Computational Infrastructure for Geodynamics, all features used are available in ASPECT version 2.4.0-pre (at aspect.geodynamics.org/), which is available at doi.org/10.5281/zenodo.6903424. The necessary parameter files to replicate models can be found at doi.org/10.5281/zenodo.8102543.

Acknowledgments

This project was funded by the National Science Foundation under award EAR-1853856. We thank the developers and the Computational Infrastructure for Geodynamics (geodynamics.org) which is funded by the National Science Foundation under award EAR-0949446 and EAR-1550901 for supporting the development of ASPECT. We also thank Portner et al. (2020) for making their tomographic model available freely, and J. Dannberg and C. Faccenna for providing comments on a thesis chapter which formed the basis for this manuscript.

521 **References**

- 522 Arnould, M., Coltice, N., Flament, N., & Mallard, C. (2020). Plate tectonics and
 523 mantle controls on plume dynamics. *Earth Planet. Sci. Lett.*, *547*, 116439.
- 524 Auth, C., Bercovici, D., & Christensen, U. R. (2003). Two-dimensional convec-
 525 tion with a self-lubricating, simple-damage rheology. *Geophys. J. Int.*, *154*,
 526 783–800.
- 527 Baes, M., Sobolev, S., Gerya, T., & Brune, S. (2020). Plume-induced subduction
 528 initiation: Single-slab or multi-slab subduction? *Geochem., Geophys., Geosys.*,
 529 *21*(2), e2019GC008663.
- 530 Bercovici, D., & Ricard, Y. (2016). Grain-damage hysteresis and plate tectonic
 531 states. *Phys. Earth Planet. Inter.*, *253*, 31–47.
- 532 Betts, P. G., Mason, W. G., & Moresi, L. (2012). The influence of a mantle plume
 533 head on the dynamics of a retreating subduction zone. *Geology*, *40*(8), 739-
 534 742.
- 535 Dalziel, I. W., Lawver, L., & Murphy, J. (2000). Plumes, orogenesis, and superconti-
 536 nental fragmentation. *Earth and Planetary Science Letters*, *178*(1-2), 1–11.
- 537 Dannberg, J., & Gassmüller, R. (2018). Chemical trends in ocean islands explained
 538 by plume–slab interaction. *Pro. Nat. Acad. Sci.*, *115*, 4351–4356.
- 539 Davies, G. F. (1986). Mantle convection under simulated plates: effects of heating
 540 modes and ridge and trench migration, and implications for the core-mantle
 541 boundary, bathymetry, the geoid and Benioff zones. *Geophys. J. R. Astr. Soc.*,
 542 *84*, 153–183.
- 543 Druken, K., Kincaid, C., Griffiths, R., Stegman, D., & Hart, S. (2014). Plume–slab
 544 interaction: the Samoa–Tonga system. *Phys. Earth Planet. Inter.*, *232*, 1–14.
- 545 Duggen, S., Hoernle, K., Hauff, F., Klügel, A., Bouabdellah, M., & Thirlwall, M. F.
 546 (2009). Flow of Canary mantle plume material through a subcontinental litho-
 547 spheric corridor beneath Africa to the Mediterranean. *Geology*, *37*, 283–286.
- 548 Enns, A., Becker, T. W., & Schmeling, H. (2005). The dynamics of subduction and
 549 trench migration for viscosity stratification. *Geophys. J. Int.*, *160*, 761–775.
- 550 Ershov, A., & Nikishin, A. (2004). Recent geodynamics of the Caucasus-Arabia-east
 551 Africa region. *Geotectonics*, *38*, 123–136.
- 552 Faccenna, C., Becker, T. W., Jolivet, L., & Keskin, M. (2013). Mantle convection in
 553 the Middle East: Reconciling Afar upwelling, Arabia indentation and Aegean

- 554 trench rollback. *Earth Planet. Sci. Lett.*, *375*, 254–269.
- 555 Fletcher, M., & Wyman, D. A. (2015). Mantle plume-subduction zone interactions
556 over the past 60 Ma. *Lithos*, *233*, 162–173.
- 557 Foley, B. J., & Becker, T. W. (2009). Generation of plate tectonics and mantle
558 heterogeneity from a spherical, visco-plastic convection model. *Geochem., Geo-*
559 *phys., Geosys.*, *10*(Q08001). doi: 10.1029/2009GC002378
- 560 Foley, B. J., & Bercovici, D. (2014). Scaling laws for convection with temperature-
561 dependent viscosity and grain-damage. *Geophys. J. Int.*, *199*, 580–603.
- 562 Fraters, M. R. T., Bangerth, W., Thieulot, C., Glerum, A. C., & Spakman, W.
563 (2019). Efficient and practical Newton solvers for nonlinear Stokes systems in
564 geodynamics problems. *Geophys. J. Int.*, *218*, 873–894.
- 565 Fuchs, L., & Becker, T. W. (2019). Role of strain-dependent weakening memory on
566 the style of mantle convection and plate boundary stability. *Geophys. J. Int.*,
567 *218*, 601–618.
- 568 Fuchs, L., & Becker, T. W. (2021). Deformation memory in the lithosphere: A com-
569 parison of damage-dependent weakening and grain-size sensitive rheologies. *J.*
570 *Geophys. Res.*, *126*, e2020JB020335.
- 571 Fuchs, L., & Becker, T. W. (2022). On the role of rheological memory
572 for convection-driven plate reorganizations. *Geophys. Res. Lett.*, *49*,
573 e2022GL099574.
- 574 Gerya, T. V., Bercovici, D., & Becker, T. (2021). Dynamic slab segmentation due to
575 brittle-ductile damage in the outer rise. *Nature*, *599*, 245–250.
- 576 Gerya, T. V., Stern, R. J., Baes, M., Sobolev, S. V., & Whattam, S. A. (2015).
577 Plate tectonics on the Earth triggered by plume-induced subduction initiation.
578 *Nature*, *527*(7577), 221–225.
- 579 Glerum, A., Thieulot, C., Fraters, M., Blom, C., & Spakman, W. (2018). Nonlinear
580 viscoplasticity in ASPECT: benchmarking and applications to subduction.
581 *Solid Earth*, *9*, 267–294.
- 582 Hager, B. H. (1984). Subducted slabs and the geoid: constraints on mantle rheology
583 and flow. *J. Geophys. Res.*, *89*, 6003–6015.
- 584 Heilman, E., & Becker, T. W. (2022). Plume-slab interactions can shut off subduc-
585 tion. *Geophysical Research Letters*, *49*, e2022GL099286.
- 586 Heister, T., Dannberg, J., Gassmüller, R., & Bangerth, W. (2017). High accuracy

- 587 mantle convection simulation through modern numerical methods – II: realistic
588 models and problems. *Geophys. J. Int.*, *210*, 833–851.
- 589 Hua, J., Fischer, K., Gazel, E., Parmentier, E., & Hirth, G. (2023). Long-distance
590 asthenospheric transport of plume-influenced mantle from Afar to Anatolia.
591 *Geochem., Geophys., Geosys.*, *24*, e2022GC010605.
- 592 Jaupart, C., Labrosse, S., Lucazeau, F., & Marechal, J.-C. (2015). Temperatures,
593 heat and energy in the mantle of the Earth. In G. Schubert (Ed.), *Treatise on*
594 *geophysics* (2nd ed., pp. 223–270). Elsevier.
- 595 Kincaid, C., Druken, K., Griffiths, R. W., & Stegman, D. R. (2013). Bifurcation
596 of the Yellowstone plume driven by subduction-induced mantle flow. *Nature*
597 *Geosc.*, *6*, 395–399.
- 598 Koppers, A. A., Becker, T. W., Jackson, M. G., Konrad, K., Müller, R. D., Ro-
599 manowicz, B., ... Whittaker, J. M. (2021). Mantle plumes and their role in
600 earth processes. *Nature Rev. Earth & Environ.*, *2*, 382–401.
- 601 Kronbichler, M., Heister, T., & Bangerth, W. (2012). High accuracy mantle convec-
602 tion simulation through modern numerical methods. *Geophys. J. Int.*, *191*, 12–
603 29.
- 604 Landuyt, W., & Bercovici, D. (2009). Formation and structure of lithospheric shear
605 zones with damage. *Phys. Earth Planet. Inter.*, *175*(115–126).
- 606 Landuyt, W., Bercovici, D., & Ricard, Y. (2008). Plate generation and two-phase
607 damage theory in a model of mantle convection. *Geophys. J. Int.*, *174*, 1065–
608 1080.
- 609 Lavier, L. L., Buck, W. R., & Poliakov, A. N. B. (2000). Factors controlling normal
610 fault offset in an ideal brittle layer. *J. Geophys. Res.*, *105*, 23431–23442.
- 611 Lay, T., Hernlund, J., & Buffett, B. (2008). Core-mantle boundary heat flow. *Nature*
612 *Geosc.*, *1*, 25–32.
- 613 Leng, W., & Zhong, S. (2008). Controls on plume heat flux and plume excess tem-
614 perature. *J. Geophys. Res.*, *113*.
- 615 Liu, L., & Stegman, D. R. (2012). Origin of Columbia River flood basalt controlled
616 by propagating rupture of the Farallon slab. *Nature*, *482*, 386–389.
- 617 Luttinen, A. V. (2018). Bilateral geochemical asymmetry in the Karoo Large Ig-
618 neous Province. *Scientific Reports*, *8*, 5223.
- 619 Mériaux, C., Duarte, J. C., Schellart, W. P., & Mériaux, A.-S. (2015). A two-way

- 620 interaction between the Hainan plume and the Manila subduction zone. *Geo-*
621 *phys. Res. Lett.*, *42*, 5796–5802. doi: 10.1002/2015GL064313
- 622 Moresi, L. N., & Solomatov, V. (1998). Mantle convection with a brittle lithosphere:
623 thoughts on the global tectonic styles of the Earth and Venus. *Geophys. J.*
624 *Int.*, *133*, 669–682.
- 625 Morishige, M., Honda, S., & Yoshida, M. (2010). Possibility of hot anomaly in
626 the sub-slab mantle as an origin of low seismic velocity anomaly under the
627 subducting Pacific plate. *Phys. Earth Planet. Inter.*, *183*, 353–365.
- 628 Navarrete, C., Gianni, G., Encinas, A., Márquez, M., Kamerbeek, Y., Valle, M.,
629 & Folguera, A. (2019). Triassic to Middle Jurassic geodynamic evolution of
630 southwestern Gondwana: From a large flat-slab to mantle plume suction in a
631 rollback subduction setting. *Earth-Science Reviews*, *194*, 125–159.
- 632 Obayashi, M., Yoshimitsu, J., & Fukao, Y. (2009). Tearing of stagnant slab. *Science*,
633 *324*, 1173–1175.
- 634 Obrebski, M., Allen, R. M., Xue, M., & Hung, S.-H. (2010). Slab-plume interaction
635 beneath the Pacific Northwest. *Geophys. Res. Lett.*, *37*(L14305). doi: 10.1029/
636 2010GL043489
- 637 Ogawa, M. (2003). Plate-like regime of a numerically modeled thermal convection in
638 a fluid with temperature-, pressure-, and stress-history-dependent viscosity. *J.*
639 *Geophys. Res.*, *108*(B2), 2067. doi: 10.1029/2000JB000069
- 640 Portner, D. E., Beck, S., Zandt, G., & Scire, A. (2017). The nature of slab slow
641 velocity anomalies beneath south america. *Geophys. Res. Lett.*, *44*(10), 4747-
642 4755.
- 643 Portner, D. E., Rodríguez, E. E., Beck, S., Zandt, G., Scire, A., Rocha, M. P., . . .
644 others (2020). Detailed structure of the subducted nazca slab into the lower
645 mantle derived from continent-scale teleseismic p wave tomography. *Journal of*
646 *Geophysical Research: Solid Earth*, *125*(5), e2019JB017884.
- 647 Pusok, A. E., & Stegman, D. R. (2020). The convergence history of India-
648 Eurasia records multiple subduction dynamics processes. *Science adv.*, *6*(19),
649 eaaz8681.
- 650 Rey, P. F., Coltice, N., & Flament, N. (2014). Spreading continents kick-started
651 plate tectonics. *Nature*, *513*, 405–408.
- 652 Ricard, Y., Richards, M. A., Lithgow-Bertelloni, C., & Le Stunff, Y. (1993). A geo-

- 653 dynamic model of mantle density heterogeneity. *J. Geophys. Res.*, *98*, 21895–
654 21909.
- 655 Ruhl, M., Hesselbo, S. P., Jenkyns, H. C., Xu, W., Silva, R. L., Matthews, K. J.,
656 ... Riding, J. B. (2022). Reduced plate motion controlled timing of Early
657 Jurassic Karoo-Ferrar large igneous province volcanism. *Science Advances*, *8*,
658 eabo0866.
- 659 Stein, C., & Hansen, U. (2013). Arrhenius rheology versus Frank-Kamenetskii
660 rheology—Implications for mantle dynamics. *Geochem., Geophys., Geosys.*, *14*,
661 2757–2770. doi: 10.1002/ggge.20158
- 662 Steinberger, B., & Calderwood, A. (2006). Models of large-scale viscous flow in the
663 Earth’s mantle with constraints from mineral physics and surface observations.
664 *Geophys. J. Int.*, *167*, 1461–1481.
- 665 Sun, D., Miller, M. S., Holt, A. F., & Becker, T. W. (2014). Hot upwelling conduit
666 beneath the Atlas Mountains, Morocco. *Geophys. Res. Lett.*, *41*, 8037–8044.
667 doi: 10.1002/2014GL061884
- 668 Tackley, P. J. (2000a). Self-consistent generation of tectonic plates in time-
669 dependent, three-dimensional mantle convection simulations 1. Pseudoplastic
670 yielding. *Geochem., Geophys., Geosys.*, *1*(1021). doi: 10.1029/2000GC000036
- 671 Tackley, P. J. (2000b). Self-consistent generation of tectonic plates in time-
672 dependent, three-dimensional mantle convection simulations 2. Strain weak-
673 ening and asthenosphere. *Geochem., Geophys., Geosys.*, *1*(1026). doi:
674 10.1029/2000GC000043
- 675 Tan, E., Gurnis, M., & Han, L. (2002). Slabs in the lower mantle and their modula-
676 tion of plume formation. *Geochem., Geophys., Geosys.*, *3*(1067). doi: 10.1029/
677 2001GC000238
- 678 Tang, Y., Obayashi, M., Niu, F., Grand, S. P., Chen, Y. J., Kawakatsu, H., ...
679 Ni, J. F. (2014). Changbaishan volcanism in northeast China linked to
680 subduction-induced mantle upwelling. *Nature Geoscience*, *7*, 470–475.
- 681 Tao, K., Grand, S. P., & Niu, F. (2018). Seismic structure of the upper mantle
682 beneath Eastern Asia from full waveform seismic tomography. *Geochem., Geo-
683 phys., Geosys.*, *19*, 2732–2763.
- 684 Ueda, K., Gerya, T., & Sobolev, S. V. (2008). Subduction initiation by thermal-
685 chemical plumes: numerical studies. *Phys. Earth Planet. Inter.*, *171*, 296–312.

- 686 van Heck, H., & Tackley, P. J. (2008). Planforms of self-consistently generated plate
 687 tectonics in 3-D spherical geometry. *Geophys. Res. Lett.*, *35*(L19312). doi: 10
 688 .1029/2008GL035190
- 689 van Hinsbergen, D. J. J., Steinberger, B., Doubrovine, P., & Gassmüller, R. (2011).
 690 Acceleration-deceleration cycles of India-Asia convergence: roles of man-
 691 tle plumes and continental collision. *J. Geophys. Res.*, *116*(B06101). doi:
 692 10.1029/2010JB008051
- 693 van Hinsbergen, D. J. J., Steinberger, B., Guilmette, C., Maffione, M., Gürer, D.,
 694 Peters, K., ... others (2021). A record of plume-induced plate rotation trigger-
 695 ing subduction initiation. , *14*, 626–630.
- 696 van Hunen, J., & van den Berg, A. P. (2008). Plate tectonics on the early Earth:
 697 limitations imposed by strength and buoyancy of subducted lithosphere.
 698 *Lithos*, *103*, 217-235.
- 699 Zhong, S. (2006). Constraints on thermochemical convection of the mantle from
 700 plume heat flux, plume excess temperature and upper mantle temperature. *J.*
 701 *Geophys. Res.*, *111*. doi: 10.1029/2005JB003972

1 Plume-driven subduction termination in 3-D mantle 2 convection models

3 **Erin Heilman^{1,2} and Thorsten W. Becker^{1,2,3}**

4 ¹Institute for Geophysics, Jackson School of Geosciences, The University of Texas at Austin, Austin TX,
5 USA

6 ²Department of Earth and Planetary Sciences, Jackson School of Geosciences, The University of Texas at
7 Austin, Austin TX, USA

8 ³Oden Institute for Computational Sciences, The University of Texas at Austin, Austin TX, USA

9 **Key Points:**

- 10 • mantle plumes can terminate subduction in 3-D, damage rheology convection
- 11 • plumes can modulate subducting slabs and plate tectonic regimes
- 12 • plume-slab interactions are plausible contributions to the Karoo-Gondwana event

Corresponding author: Erin Heilman, eheilman@lanl.gov

Abstract

The effect of mantle plumes is secondary to that of subducting slabs for modern plate tectonics, e.g. when considering plate driving forces. However, the impact of plumes on tectonics and planetary surface evolution may nonetheless have been significant. We use numerical mantle convection models in a 3-D spherical chunk geometry with damage rheology to study some of the potential dynamics of plume-slab interactions. Substantiating our earlier work which was restricted to 2-D geometries, we observe a range of interesting plume dynamics, including plume-driven subduction terminations, even though the new models allow for more realistic flow. We explore such plume-slab interactions, including in terms of their geometry, frequency, and the overall effect of plumes on surface dynamics as a function of the fraction of internal to bottom heating. Some versions of such plume-slab interplay may be relevant for geologic events, e.g. for the inferred ~ 183 Ma Karoo large igneous province formation and associated slab disruption. More recent examples may include the impingement of the Afar plume underneath Africa leading to disruption of the Hellenic slab, and the current complex structure imaged for the subduction of the Nazca plate under South America. Our results imply that plumes may play a significant role not just in kick-starting plate tectonics, but also in major modifications of slab-driven plate motions, including for the present-day mantle.

Plain Language Summary

Subduction of cold, strong lithospheric slabs is the main plate driving force within mantle convection. However, hot upwellings, mantle plumes, may have a greater role in modulating plate motions and slab trajectories than previously thought. We use 3-D numerical convection models that account for the weakening of rocks due to the accumulation of deformation to understand the effect that mantle plumes can have on subduction zones. We show that plumes can terminate subduction in a range of circumstances. We also test the effect of the amount of internal heating compared to heat from the core which is the major convective control on the importance of plumes. We discuss cases where these plume-slab terminations may have occurred on Earth, in the geological past, and for the present day through plate reconstructions and consideration of seismic tomography.

1 Introduction

Subduction of the cold, lithospheric boundary layer is the main driving force of plate tectonics through slab pull due to temperature-dependent viscosity and the dominance of internal heating in mantle convection. However, there is also feedback between subducting slabs and mantle plumes as long as there is some degree of bottom heating. While instabilities of the bottom thermal boundary layer can form plumes anywhere, a perturbation, for instance due to a subducting slab, will affect the timing and location for the formation of mantle plumes (e.g. Tan et al., 2002; Dannberg & Gassmüller, 2018; Arnould et al., 2020). This phenomenon suggests a possible feedback, or “talk-back”, between plumes and slabs. Hence, when mantle plumes reach the top thermal boundary layer, i.e. the lithosphere, they too can perturb the cold thermal boundary layer, e.g. creating hotspot volcanics and large igneous provinces (LIPs), contributing to rifting and supercontinental breakup, subduction initiation, and contributing to a low viscosity asthenosphere (e.g. Koppers et al., 2021). When plumes reach the lithosphere at a subduction zone they can interact with slabs by temporarily speeding up plates (van Hinsbergen et al., 2011; Puskok & Stegman, 2020), affecting trench motion and convergence rates (Betts et al., 2012; Mériaux et al., 2015), being deflected by slabs (Druken et al., 2014; Kincaid et al., 2013), or disrupting slabs (Liu & Stegman, 2012; Heilman & Becker, 2022).

Such plume-slab disruption has been less well explored because one may expect a strong, thick slab to survive any plume-induced deformation. As a consequence, when discussing plume-slab interactions, most think of plumes as a possible driver to initiate subduction, and plume-affected plate tectonics has been explored in several models. Plumes may kick-start subduction either directly or by means of emplacing surface density contrasts (Ueda et al., 2008; Rey et al., 2014; Gerya et al., 2015; Baes et al., 2020), and plume induced modification of plate speeds may lead to far field forces for subduction initiation (van Hinsbergen et al., 2021).

However, if strain-dependent damage rheologies, e.g. akin to those explored by Gerya et al. (2021) implemented in simplified form following Fuchs and Becker (2021), are accounted for, plumes do in fact appear capable of terminating subduction as well (Heilman & Becker, 2022). This process can also be associated with an interesting feedback loop of subducting slabs initiating mantle plumes at the core–mantle boundary, plumes terminating subduction close to the surface after their ascent through the mantle, and the

75 broken-off slabs descending through the mantle to possibly begin the process again. While
76 this would, of course, be just one aspect of the time-dependent convection system includ-
77 ing possibly episodic or irregular plate tectonic motions, it is one interaction loop that
78 leaves possibly diagnostic traces in rock record. For example, Fletcher and Wyman (2015)
79 identified that in the past 60 Ma, 18 plumes have been within 1000 km of subduction
80 zones, which points to plume-slab interactions, and potential terminations, as a relevant
81 process to consider for the evolution of the plate tectonic system. Heilman and Becker
82 (2022) explored the effects of internal heating, and thickness, or average temperature/age,
83 of slabs as controlling factors for the likelihood of plumes terminating slabs and mod-
84 ifying the overall tectonic regime, such as a transition from plate-tectonics to stagnant
85 lid. However, our earlier work was limited to 2-D, and one may rightly ask if such a re-
86 striction of flow is a precondition for plume-slab termination.

87 Investigating the nature of plume-slab termination in 3-D is both more realistic and
88 more challenging. For the present-day mantle, we appear to mainly see plume-slab in-
89 teractions where plumes are taking advantage of existing slab windows or tears, formed
90 by plate reorganizations or local slab dynamics (Obrebski et al., 2010; Betts et al., 2012;
91 Portner et al., 2017, 2020). Previously, Betts et al. (2012) showed based on 3-D mod-
92 eling that a plume could modulate subduction in the case of trench rollback causing a
93 subducting slab to move over a plume head. In this instance, a slab window was formed
94 and subduction continued once the slab rolled completely over the plume head.

95 Investigations of suggested recent plume advance include the case of Canary to-
96 ward the Alboran slab underneath the Atlas mountains (Duggen et al., 2009; Sun et al.,
97 2014; Mériaux et al., 2015) and Afar toward Anatolia and the Hellenic subduction zone
98 (Ershov & Nikishin, 2004; Faccenna et al., 2013; Hua et al., 2023). Present-day settings
99 include the Yellowstone/Farallon case (Obrebski et al., 2010; Liu & Stegman, 2012) and
100 the South American Juan de Fuca plume-slab window (Portner et al., 2017, 2020). These
101 studies point to the lithosphere, e.g. in terms of slab tears or windows during trench roll-
102 back, or delamination, being the dominant control, and mantle plumes being secondary
103 to lithosphere dynamics. Plume-slab termination in 3-D will depend on the lateral ex-
104 tents necessary for the interaction to cover, and thermo-mechanical heterogeneity of the
105 mantle and crust. In particular, subduction termination can potentially become easier
106 when damage rheologies or other tectonic inheritance leads to weakening of slabs, includ-

107 ing by segmentation and tears (van Hunen & van den Berg, 2008; Betts et al., 2012; Gerya
108 et al., 2021).

109 Here, we model 3-D, mantle convection in a spherical “chunk” geometry with dam-
110 age rheology and a mixed heating regime similar to Earth’s convective vigor. We explore
111 how damage rheology affects plume-slab interactions and show that plume-induced slab
112 termination is indeed possible in 3-D. We discuss possible instances where this may have
113 happened from the geologic record and present-day seismic tomography to relate our nu-
114 merical models to the Earth.

115 2 Model Setup

116 To model mantle convection as a fluid convection problem in the infinite Prandtl
117 number and incompressible, Boussinesq approximation, we can express conservation of
118 momentum and mass as

$$119 \quad -\nabla \cdot [2\eta\varepsilon(\mathbf{u})] + \nabla p = \rho\mathbf{g} = \rho_0\alpha(T - T_{ref}) \quad (1)$$

$$120 \quad \nabla \cdot \mathbf{u} = 0, \quad (2)$$

122 and conservation of energy without shear heating as

$$123 \quad \rho C_p \left(\frac{\partial T}{\partial t} + \mathbf{u} \cdot \nabla T \right) - \nabla \cdot k \nabla T = \rho H, \quad (3)$$

124 while allowing for advection of a compositional or general tracer field c

$$125 \quad \frac{\partial c}{\partial t} + \mathbf{u} \cdot \nabla c = 0. \quad (4)$$

126 Here, ε is the strain-rate tensor, \mathbf{u} velocity, p pressure, g gravity, T temperature, ρ den-
127 sity, with a reference of ρ_0 at T_{ref} , C_p specific heat capacity, k thermal conductivity, H
128 the internal heat production, η viscosity, α thermal expansivity, and c composition. Eqs. (1)
129 and (2) capture laminar Stokes flow, driven by thermal body forces, and eq. (3) describes
130 the temperature field that is diffused and advected with the flow velocity \mathbf{u} , where the
131 right-hand term is internal heat production. Eq. (4) governs how diffusion-free compo-
132 sitional fields evolve over time; in our models the compositional field tracked is a pas-

133 sive, effective “strain” property used to approximate damage evolution, as in Fuchs and
 134 Becker (2019, 2021), and does not involve additional, e.g., density contributions.

135 To solve eqs. (1-4), we use the open-source, finite element mantle convection code
 136 *ASPECT* (Kronbichler et al., 2012; Heister et al., 2017; Fraters et al., 2019). Our ap-
 137 proach overall follows that of Heilman and Becker (2022), but we employ a Newtonian,
 138 Frank-Kamenetskii linearized temperature-dependent viscosity law (cf. Tackley, 2000a;
 139 Stein & Hansen, 2013) to simplify the model for a 3-D test case. The equation is as fol-
 140 lows,

$$141 \quad \eta(T) = \eta_{ref} \exp \left[\frac{E}{1 + \frac{T}{T_{ref}}} - \frac{E}{2} \right] \quad (5)$$

142 where η_{ref} is a reference viscosity, E is a non-dimensional activation energy, and T_{ref}
 143 is a reference temperature. Added into this viscosity law is a viscosity jump at 660 km
 144 depth, where the η_{ref} is increased by a factor of 30 in the lower mantle, as expected from
 145 geoid modeling and slab sinking rates (e.g. Hager, 1984; Ricard et al., 1993; Steinberger
 146 & Calderwood, 2006).

147 Additionally, we include visco-plasticity and a simplified damage rheology in our
 148 models (e.g. Tackley, 2000b; Ogawa, 2003; Auth et al., 2003; Fuchs & Becker, 2019). *AS-*
 149 *PECT* employs plasticity and a possible strain-weakening for modulating the yield stress
 150 (Glerum et al., 2018). When the viscous stress ($2\eta\dot{\epsilon}_{II}$) exceeds the yield stress the vis-
 151 cosity is rescaled back to an effective yield viscosity (e.g., Moresi & Solomatov, 1998; Enns
 152 et al., 2005).

$$153 \quad \eta_{eff} = \frac{\sigma_y}{2\dot{\epsilon}_{II}}. \quad (6)$$

154 We then use a strain-based damage variable γ to reduce the yield stress from the back-
 155 ground value (e.g. Lavier et al., 2000; Ogawa, 2003). Damage, γ , evolves according to

$$156 \quad \frac{d\gamma}{dt} = \dot{\epsilon}_{II} - \gamma A_d \cdot \exp [E_d (T - T_0)] \quad (7)$$

157 where $\dot{\epsilon}_{II}$ is the second invariant of the strain-rate tensor, A_d is a timescale for strain-
 158 healing, E_d is a non-dimensional activation energy, following temperature- and time-dependent
 159 strain healing (Fuchs & Becker, 2019). Combining plasticity and such a damage rheol-
 160 ogy, which incorporates strain-weakening and strain-healing, can approximate the be-
 161 havior of physical weakening processes like those inferred from grain-size dependent rhe-

Table 1. Model parameters

Parameter	Value
Temperature difference between thermal boundary layers	2373 K
Density ρ	3700 kg/m ³
Thermal expansivity α	$2 \cdot 10^{-5}$ K ⁻¹
Thermal diffusivity κ	10^{-6} m ² /s
Specific heat capacity C	750 J/gK
Internal heating rate H	$5.0 \cdot 10^{-12}$ W/kg
Minimum viscosity η_{min}	10^{18} Pas
Maximum viscosity η_{max}	$2.5 \cdot 10^{24}$ Pas
Non-dimensional activation energy E	29.95
Reference viscosity η_{ref}	$4.5 \cdot 10^{19}$
Reference temperature for viscosity T_{ref}	2500 K
Yield stress for Damage Model	140 MPa
Minimum weakened yield stress for Damage Model	35 MPa
Yield stress for No Damage Model	55 MPa
Non-dimensional strain weakening factor s.w.f.	0.25
Non-dimensional activation energy for strain healing E_d	250
Non-dimensional timescale for strain healing A_d	10^{-7}

162 ologies (Fuchs & Becker, 2021), which is one of the suggested mechanisms for strain lo-
163 calization (e.g. Landuyt & Bercovici, 2009; Bercovici & Ricard, 2016). The strain-weakening
164 factor (Table 1) is set to reduce the yield stress linearly by 75%, i.e. from 140 to 35 MPa,
165 with parameters based on our earlier work. This accumulation/healing formulation al-
166 lows damage to persist and be advected in cold lithosphere while damage in the man-
167 tle is healed according to a specified rate with temperature (Table 1). We compare a model
168 with damage rheology to a model without to understand the effect of damage on the abil-
169 ity of mantle plumes to terminate subduction.

171 Temperature boundary conditions for our mixed heating convection model are 273 K
172 and 2573 K for the surface and core-mantle boundary, respectively, and the mechani-
173 cal boundary conditions are free slip on all sides. We use a reference internal heating value
174 of $5 \cdot 10^{-12}$ W/kg (Table 1) and compare the effect of different internal heating produc-
175 tion rates in subsequent models. The Earth's ratio of internal to bottom heating is in-
176 completely constrained and expected to be time-variable over planetary history because
177 of the decay of radiogenic material. We expect the balance of bottom to internal heat-
178 ing to control the relative importance of mantle plumes from a general understanding
179 of mantle convection (e.g. Davies, 1986; Zhong, 2006; Leng & Zhong, 2008; Foley & Becker,
180 2009) and our earlier, 2-D tests (Heilman & Becker, 2022).

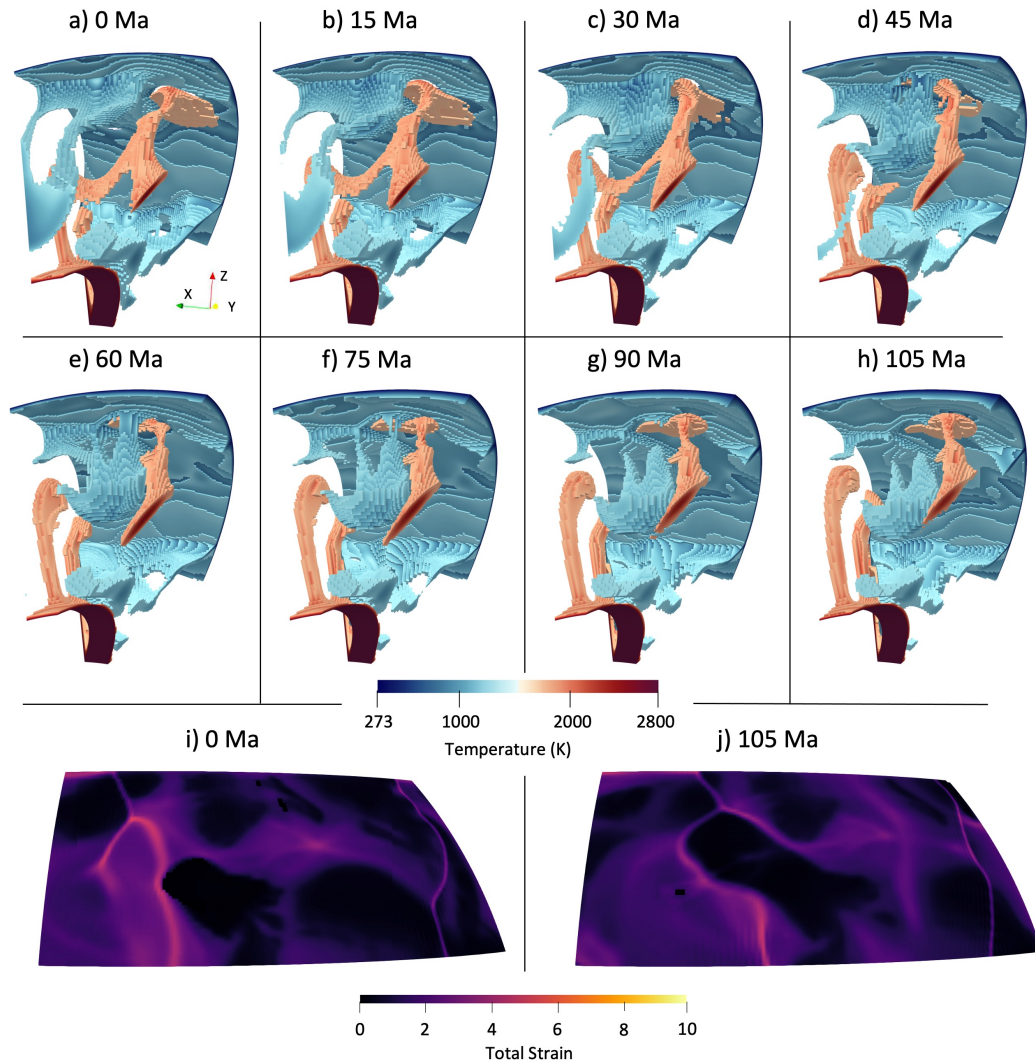
181 We compare our reference model with a non-damage rheology case, which requires
 182 a lower yield stress to roughly match the convective vigor of the models with damage
 183 (cf. Fuchs & Becker, 2022). The effective Rayleigh number of our reference computation
 184 is $\sim 3.5 \cdot 10^6$. Bulk metrics such as surface heat flow are in Earth-like ranges (sec. 3.3),
 185 with surface velocities ~ 3 times lower than for present-day plate speeds. We thus ex-
 186 pect the dimensionalized model times to broadly correspond to actual time for our ref-
 187 erence models. However, to make models with different parameters and hence convec-
 188 tive vigor overall comparable, e.g., in terms of frequency of tectonic events, we also re-
 189 port times in units of overturn time, i.e. the typical time taken for a density anomaly
 190 to traverse the mantle and back. For the Earth, those can be converted by multiplying
 191 with relevant timescales, ~ 300 Myr for ~ 2 cm/yr average vertical motions.

192 **3 Results**

199 **3.1 Damage Rheology Model**

200 We first explore a model with the damage rheology and a yield stress of 140 MPa
 201 (Figure 1) building on the work by Heilman and Becker (2022). Including damage rhe-
 202 ology in a convection model leads to potential localization of deformation, formation of
 203 persistent weak zones (e.g. Auth et al., 2003; Landuyt et al., 2008), as well as possibly
 204 an overall drop in bulk lithospheric strength, e.g. if damage reduces the yield stress (cf.
 205 Foley & Bercovici, 2014; Fuchs & Becker, 2019, 2022). In our models, the damage rhe-
 206 ology weakens the subducting slabs and allows the weakness to persist because the slabs
 207 are cold. When mantle plumes strike the lithosphere, the damage is reduced as the plumes
 208 introduce heat. This can lead to the healing effect to take over, reducing the associated
 209 inherited weak zones on the surface. This does not mean that plumes make the litho-
 210 sphere strong in our models, they still tend to decrease the viscosity of the lithosphere
 211 that they underplate, and generally lead to some mode of extension on the surface.

212 To visualize the plume-slab interactions and terminations we applied a tempera-
 213 ture threshold for both the mantle plumes and subducting slabs. This thresholding al-
 214 lowed us to visualize features and interactions easily in 3-D. Figure 1a-h shows the tem-
 215 perature thresholding on the left for a plume-slab termination event. The total accumu-
 216 lated strain on the surface in Figure 1i-j shows the influence of the hot plume on the sub-
 217 duction zone in terms of damage. As the plume terminates subduction, the damage that



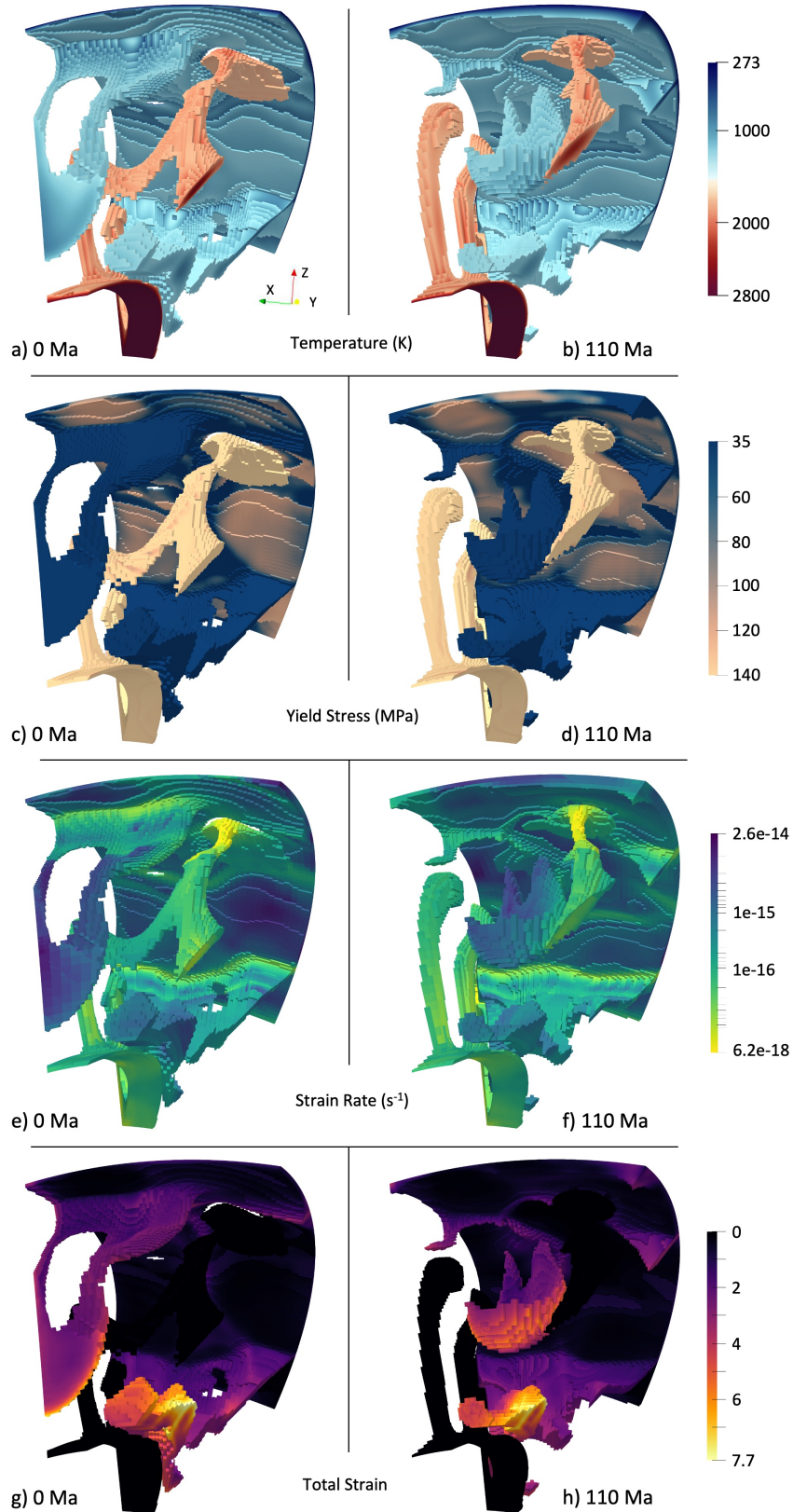
193 **Figure 1.** Example of a rising mantle plume terminating an subduction zone in 3-D for our
 194 reference model with damage. a-h show temperature thresholds of plumes (~ 1750 - 2773 K, red
 195 colors) and slabs (273 - ~ 1250 K, blue) over several timesteps showing a plume-slab interactions.
 196 Plots i-j show the damage, expressed as effective “strain”, at the surface at the first and last
 197 timestep. When the plume strikes the surface, it resets the damage and it influences the subduc-
 198 tion zone to bend around it.

218 was accumulated in the subduction zone in the lithosphere (Figure 1i) deflects around
219 where the plume head strikes the lithosphere (Figure 1j), because the plume head intro-
220 duces heat to the lithosphere which then increases the amount of strain healed above the
221 plume. This configuration of damage remains frozen in the lithosphere and is advected
222 along the surface until a new subduction zone is initiated from the damaged arc (cf. Fo-
223 ley & Bercovici, 2014; Fuchs & Becker, 2019; Heilman & Becker, 2022).

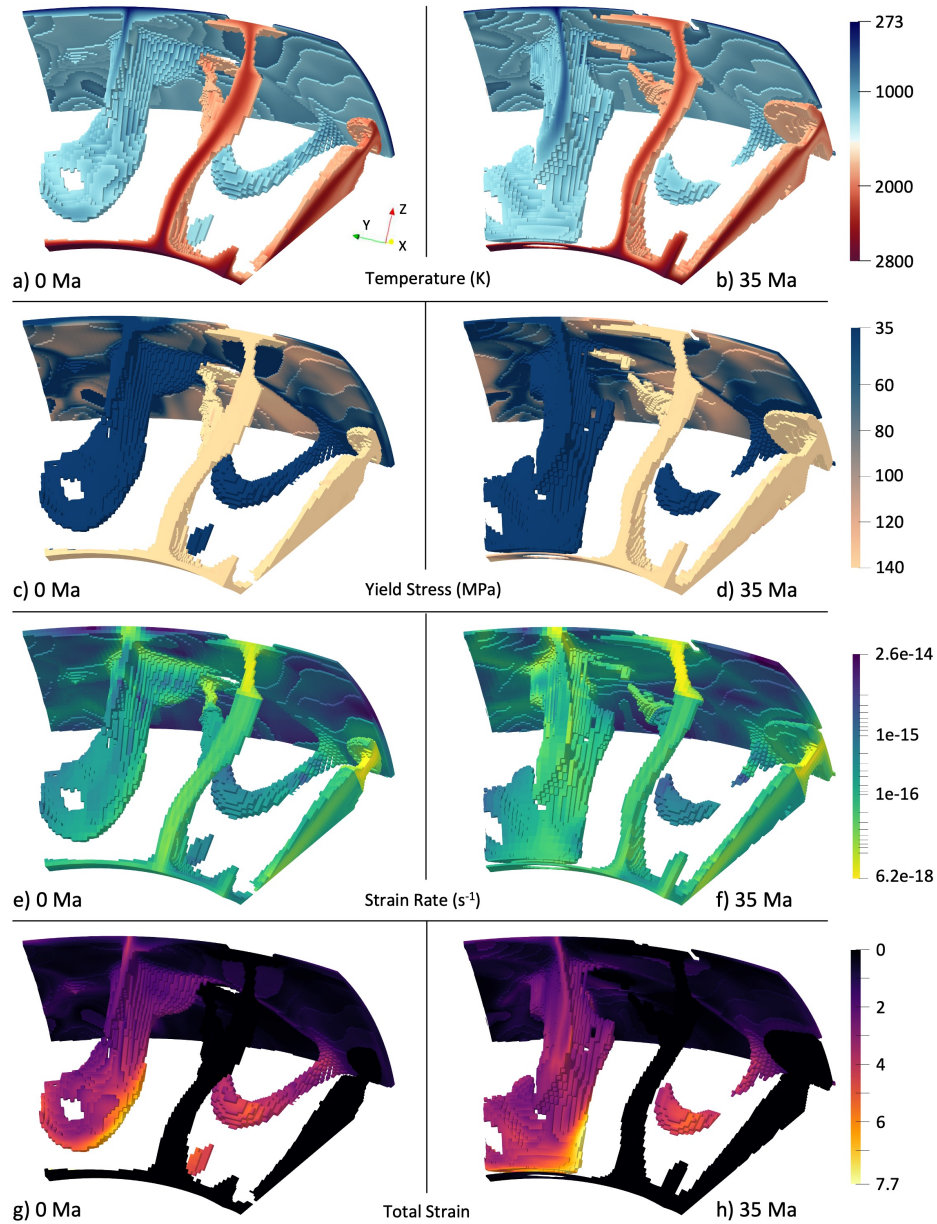
224 The reference model ran for a total of 3 model overturns, beginning from an ini-
225 tial steady state model run. During the qualifying model run time of 3 overturns, we ob-
226 serve 7 instances of plume-slab termination, i.e. an average of 2.3 terminations every over-
227 turn. In these models, termination of subduction is quantified through the temperature
228 thresholding when no part of the subducting slab is connected to the trench of the sub-
229 duction zone. These termination events do not tend to overlap in time, however we do
230 observe an instance when two terminations are present at the same time. Terminations
231 are clustered in time, with periods of quiescence, similar to what was observed and an-
232 alyzed by Heilman and Becker (2022).

233 Six of the seven termination events occurred with a single plume impinging on a
234 subduction zone causing the termination. The six events do vary in where the plume in-
235 teracts with the slab along its lateral extent. If the plume strikes the center of the sub-
236 ducting slab, the termination tends to develop by creating a slab window that then ex-
237 tends along the length of the slab until it is fully terminated (as in Figure 1). If the plume
238 head interacts with the slab closer to the subducting slabs lateral extent, then the ter-
239 mination has an unzipping effect as the slab begins detaching at the plume head and con-
240 tinues along the length of the slab. The last termination was caused by two plumes on
241 both sides of the subduction zone that pinched out the subducting slab to shut off sub-
242 duction.

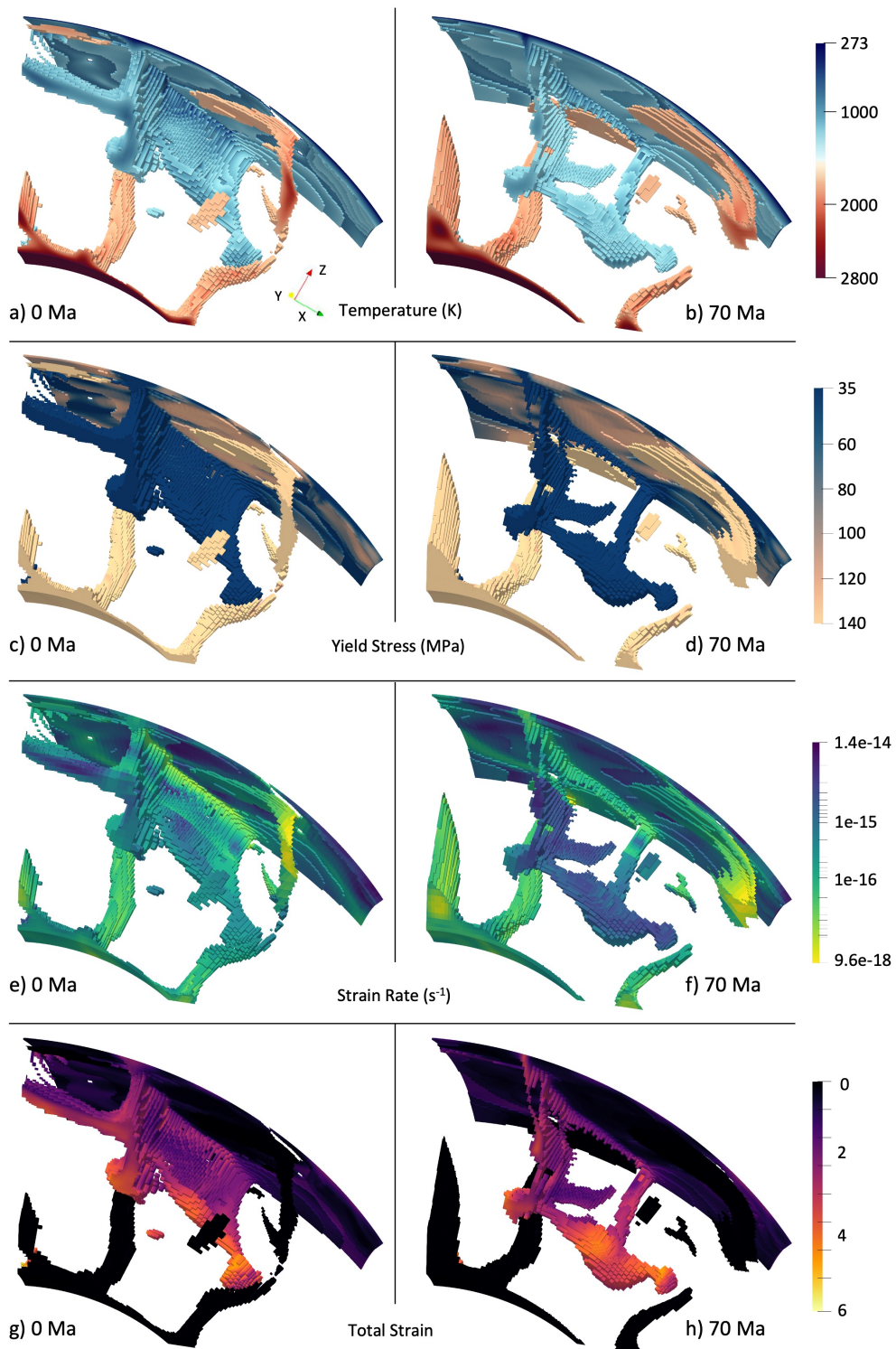
252 Figures 2, 3, and 4 show these styles of termination in temperature, yield stress,
253 strain rate, and total strain (accumulated damage) before and after termination, where
254 termination is inferred from the visualization as the time when the slab is fully detached.
255 We observe in these terminations that the subducting slab is strongly weakened during
256 subduction, while the mantle plume is not further weakened by damage or plasticity, due
257 to its inherent higher temperature (cf. Fuchs & Becker, 2019). Both the mantle plume
258 and the subducting slab, in the area of the most bending in the slab, have high strain



243 **Figure 2.** Temperature, yield stress, strain rate, and accumulated strain (damage) before (a,
 244 c, e, g) and after termination (b, d, f, h) for a typical termination (same termination as Figure 1)
 245 where a plume impinges on a subducting slab and shuts off subduction.



246 **Figure 3.** Temperature, yield stress, strain rate, and accumulated strain (damage) before (a,
 247 c, e, g) and after termination (b, d, f, h) for a termination where a plume impinges on the edge of
 248 a subducting slab and shuts off subduction by unzipping along the slab's length.



249 **Figure 4.** Temperature, yield stress, strain rate, and accumulated strain (damage) before (a,
 250 c, e, g) and after termination (b, d, f, h) for a double-sided termination where two plumes pinch
 251 out a subducting slab to shut off subduction.

259 rates that lessen after termination has occurred. In the case of damage, the subducting
 260 slabs have a moderate (~ 2 -5) amount of accumulated damage. This is a result of the weak-
 261 ening and slow healing in the cool slab, as opposed to the hot mantle plumes that have
 262 no accumulated damage. After termination occurs, the damage persists in the terminated
 263 slab as it sinks in the mantle, until the slab is heated enough that the damage is healed
 264 (cf. Fuchs & Becker, 2019).

265 However, as may be expected, and explored more fully in 2-D (Heilman & Becker,
 266 2022), not every plume-slab interaction ends in a termination. We find at least five in-
 267 stances where a plume interacts with a subducting slab without causing a complete ter-
 268 mination, i.e. a roughly 60% chance of plumes shutting down subduction if they get close
 269 to slabs, for our chosen parameter values. Some of these plume-slab interactions result
 270 in no change to the subducting slab morphology from the plume. While in some cases,
 271 the plume creates a slab window in the subducting slab but subduction is able to con-
 272 tinue normally, as has been suggested for modern settings based on seismic tomography.

273 **3.2 Non-Damage Rheology Model**

274 We include a model without the damage rheology to compare to the plume-slab
 275 interactions we observe in the damage model. In this non-damage model, the background
 276 yield stress has to be lowered to 55 MPa from 140 MPa to achieve the same convective
 277 vigor and maintain a mobile convective regime (comparable Rayleigh number of $\sim 3.8 \cdot 10^6$).
 278 Both of the used yield stress values are required to achieve plate-like motions with a mo-
 279 bile lid in our models, however, the values are much smaller than what would be expected
 280 from rock mechanics. This is a typical finding for visco-plastic, plate-like convection mod-
 281 els (e.g. Moresi & Solomatov, 1998; van Heck & Tackley, 2008; Foley & Becker, 2009),
 282 and might indicate some additional weakening mechanism, such as hydration. However,
 283 our point here is not about the absolute values, but we merely provide an attempt to
 284 compare damage and no-damage cases at similar convective vigor and tectonic style.

285 Our non-damage model has a total run time of ~ 6 overturns, and this model showed
 286 only one example of plume-slab termination. In this termination, a plume first formed
 287 a slab window in a subducting slab, which then caused a slab tear on either side of the
 288 slab window, and lead to the eventual termination of the subduction zone. There were
 289 four other instances where a mantle plume caused the formation of a slab window that

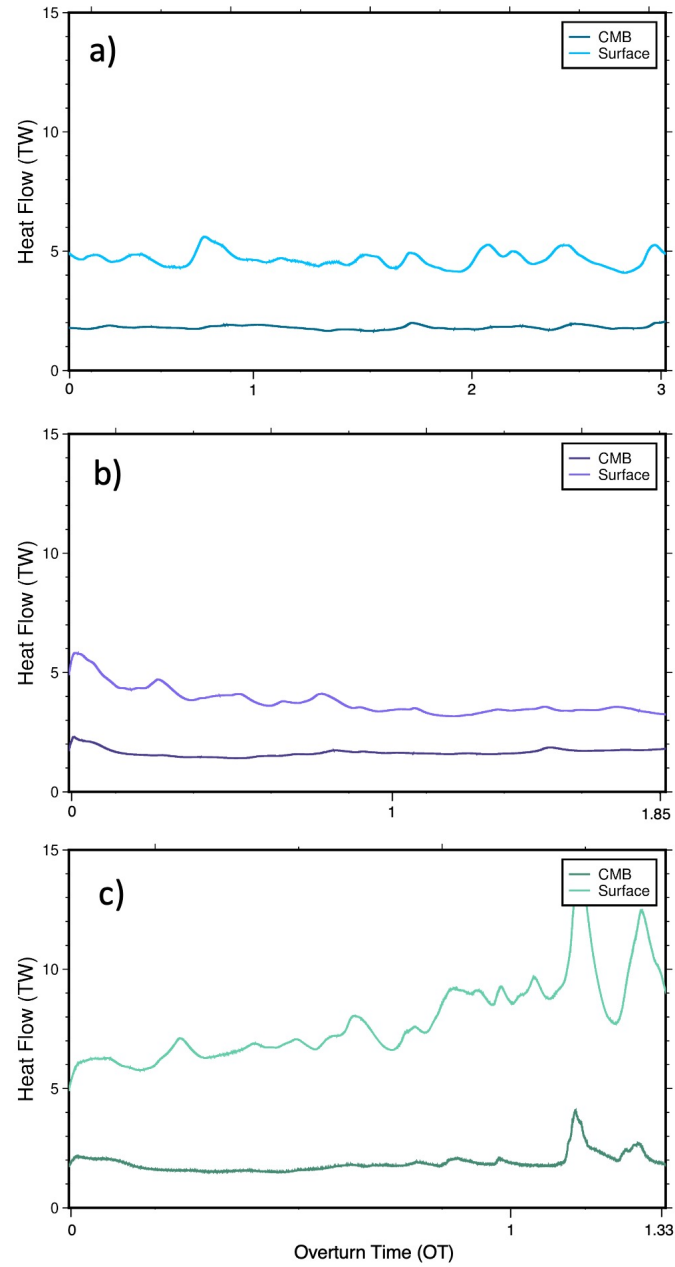
290 did not result in an immediate termination of subduction. In this non-damage rheology
 291 case, the yield stress in the subducting slab can be higher than that in the damage rhe-
 292 ology case due to the lack of weakening. This higher slab yield stress is likely why we
 293 see more formations of slab windows than full plume-slab terminations in our non-damage
 294 model.

295 **3.3 Ratios of Internal Heating**

296 We expect the amount of internal heating to affect the importance of plumes, which
 297 are trivially absent if there is no bottom heating, and whose effect will be maximal for
 298 pure bottom heating. To compare our reference damage rheology results, two other mod-
 299 els were run with a lower ($5 \cdot 10^{-13}$ W/kg) and a higher ($2 \cdot 10^{-11}$ W/kg) amount of
 300 internal heat production, i.e. 0.1 and 4 times the heat production of the initial damage
 301 rheology model. The heat flow time series for the three models are shown in Figure 5.
 302 The average heat flow for the reference model (Figure 5a) is 1.81 TW for the core-mantle
 303 boundary (CMB) and 4.69 TW for the surface. The relative contribution of 61.5% from
 304 internal heating for the reference model is in the ballpark of estimates for the Earth's
 305 mantle (Leng & Zhong, 2008; Lay et al., 2008; Jaupart et al., 2015), which are, however,
 306 uncertain. The average heat flow for the lower heating model (Figure 5b) is 1.67 TW
 307 out of the CMB and 3.77 TW out of the surface, for 55% contribution from internal heat-
 308 ing. The average heat flow for the higher heating model (Figure 5c) is 1.76 TW out of
 309 the CMB and 7.27 TW out of the surface, for 75% contribution from internal heating.

310 Considering absolute values, our 3-D spherical chunk is roughly 15% of the surface
 311 area of the Earth. Scaling the heat flow out of the surface of the model to Earth would
 312 be roughly 31.3 TW for the reference model, and 25.1 TW and 48.5 TW for the lower
 313 and higher heating model, respectively. These values are comparable to estimates for the
 314 convective heat flow of the mantle, ~ 38 TW (Jaupart et al., 2015). This implies that while
 315 our focus here is, of course, mainly to explore the general controls on plume dynamics,
 316 and we did not account for secular cooling, the overall convective vigor of the models may
 317 be comparable to the mantle.

320 While having only changed the internal heat production, complexities arise because
 321 different average viscosities result via the temperature-dependent creep laws used. This
 322 means that these models have different Rayleigh numbers, or convective vigor, with es-



318 **Figure 5.** Heat flow out of the CMB and surface are plotted over overturn times for three
 319 models. a) Damage Model. b) Lower Internal Heating Model. c) Higher Internal Heating Model.

323 timates for the Rayleigh numbers $4.65 \cdot 10^5$, $9.95 \cdot 10^6$, and $7.16 \cdot 10^7$ for the lower, ref-
324 erence, and higher heating cases, respectively. This changing convective vigor does have
325 an effect on the planform of convection. However, these models all remain predominantly
326 mobile and in a plate tectonic-like convection regime, meaning they should be broadly
327 comparable in terms of their dynamics, including plume-slab interactions.

328 The model with a lower proportion of heating ran for a total of 1.85 overturns from
329 an initial steady state model. This model showed eleven plume-slab terminations, i.e.
330 roughly 5 per overturn. These terminations follow the same trend as in the reference model,
331 where the subducting slab is fully weakened before the termination, strain rate is high
332 in both the slab and plume and lessens after termination, and the subducting slab is dam-
333 aged prior to termination. We also see in this model a non-termination event creating
334 a slab window in the subducting slab and subduction continues. Specifics of these in-
335 teractions and the detailed numbers of terminations per a given typical model time are,
336 of course, subject to stochastic fluctuations.

337 The model with a higher proportion of heating had a total run time of 1.33 over-
338 turns after starting from an initial steady state model. This model showed two plume-
339 slab terminations, i.e. ~ 1.5 terminations per one overturn. This model had hotter av-
340 erage mantle temperatures (2034 K compared to the reference model 1518 K) and there-
341 fore hotter subducting slab temperatures due to the increased proportion of internal heat-
342 ing. It was more difficult to identify instances when plumes were actively shutting off
343 subduction as the hotter mantle led to the subducting slabs warming quickly and de-
344 taching even without plume influence. The model becomes unstable towards the end of
345 its run time and moves into an episodic regime (as seen in Figure 5c) and may be more
346 relevant for ealy Earth rather than, say, Cenozoic mantle convection (e.g. van Hunen &
347 van den Berg, 2008).

348 Given variations in the relative importance of bottom and internal heating, we thus
349 find the expected effect on the rate of plume-slab terminations per overturns. All mod-
350 els show plume-slab terminations and interactions, but for the lower internal heating model
351 the frequency of plume-termination events was almost double the reference model. The
352 opposite is true for the higher internal heating model with fewer plume driven subduc-
353 tion terminations, substantiating the 2-D results of Heilman and Becker (2022). We also
354 ran two other models with intermediate heat production of $8 \cdot 10^{-12}$ W/kg and $1 \cdot 10^{-11}$ W/kg

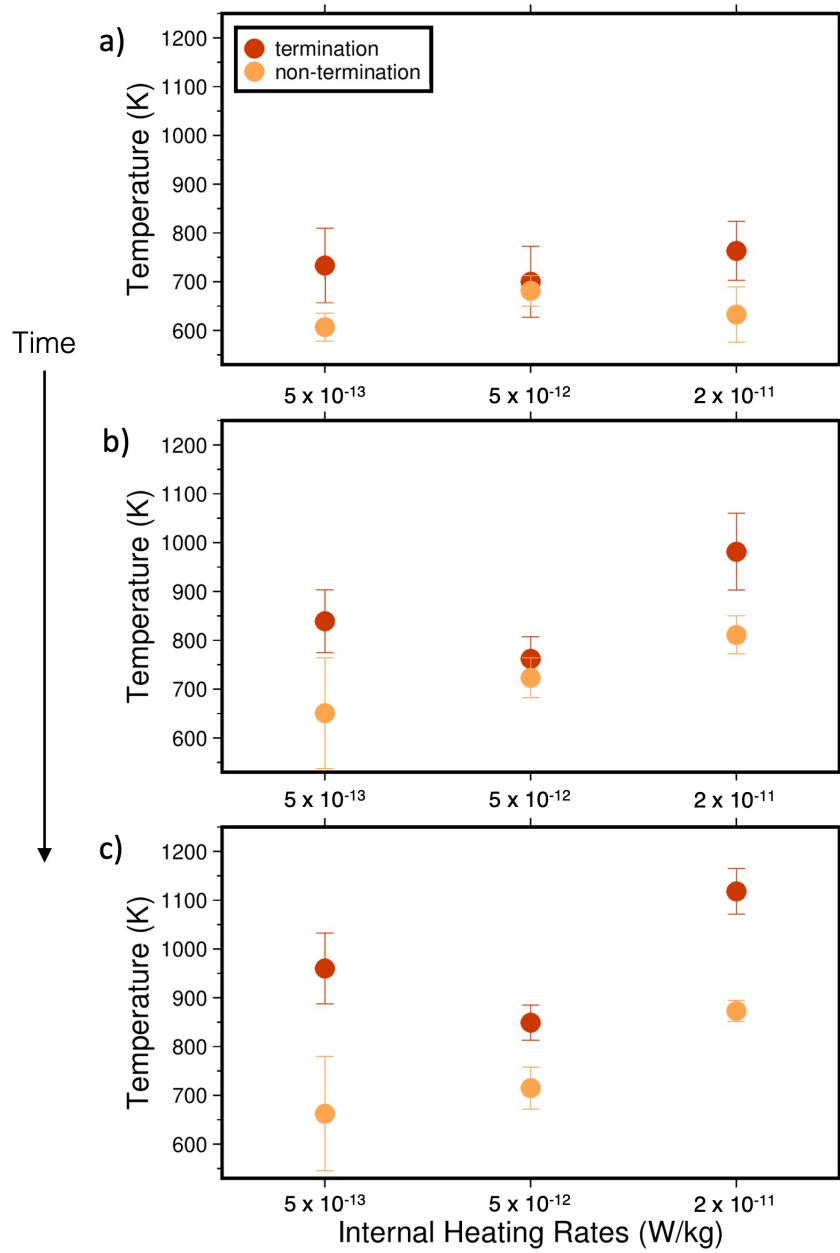
355 for validation and the termination numbers were in between the higher heat model and
356 the reference model.

357 Due to the additional degrees of freedom provided by 3-D flow compared to the anal-
358 ysis of Heilman and Becker (2022), and the highly time-dependent nature of the convec-
359 tive system, further, systematic analysis of controlling factors beyond the overall effect
360 of internal heating has to be somewhat limited. We measured internal slab temperature
361 for both terminating and non-terminating plume-slab interactions by sampling temper-
362 atures from the subducting slab for a period of 60 Ma (well within the overall termina-
363 tion and interaction times). The temperatures were collected over a 50 km section of the
364 subduction zone where the plume was actively interacting with it, at a spacing of 10 km
365 intervals. These data were averaged over the length (50 km) and the standard deviation
366 was taken to show the variability of temperature within the slab. In general, we find that
367 the non-terminating interactions are typically happening for slabs that are colder and
368 hence thicker, as expected (Heilman & Becker, 2022).

372 We plot slab temperatures for terminations and non-terminations as a function of
373 internal heating in Figure 6. As the average mantle temperature increases, plumes con-
374 tribute less to the convective dynamics, so there are less terminations overall. For these
375 models, the respective average mantle temperatures are 1278, 1518, and 2034 K. The age
376 of thickness of the subducting slab as reflected in our temperature estimates during non-
377 terminations follows this trend as well, shown most clearly in Figure 6c where the non-
378 termination temperatures increase with the proportion of internal heating.

379 **4 Discussion**

380 Our models show that plume-driven subduction terminations occur in 3-D spher-
381 ical geometry convection models, substantiating the suggestion of Heilman and Becker
382 (2022). This implies that plume-induced subduction termination may indeed happen on
383 Earth, if convective vigor and actual rock rheology are similar to those represented by
384 our model. A prerequisite for termination is that the slab can be weakened, as is the case
385 for our damage rheology model. While slab pull forces can be supported for plate-like
386 motions even in the presence of weakening (cf. Gerya et al., 2021), the accumulated dam-
387 age makes it easier for the mantle plume to cut through, or pinch out, the subducting
388 slab (Figures 2, 3, and 4). While it is perhaps becoming more broadly accepted that the



369 **Figure 6.** Subducting slab temperatures for terminations and non-terminations for each ratio
 370 of internal heating. Plots a), b), and c) increase in 20 Ma time increments showing the trend in
 371 slab temperature over time for each internal heating ratio.

389 lithosphere is significantly weakened in the trench region where the plate is bending, our
390 rheological choices may, of course, lead to slabs that are weaker than in the Earth's man-
391 tle. However, since slab segmentation is a widely inferred process (e.g. Tan et al., 2002;
392 Liu & Stegman, 2012), we would expect plume-slab terminations for stronger slabs to
393 be perhaps less frequent on Earth than in our models, rather than being completely ab-
394 sent.

395 Besides rheology, the other control on the importance of plume-slab interactions
396 is the degree of bottom to internal heating. Our results for a higher to lower rate of in-
397 ternal heating (sec. 3.3 and Figure 6) could be interpreted as being indicative of the evo-
398 lution of mantle dynamics from the early Earth to present-day. As the internal heating
399 of the mantle has decreased by a factor of ~ 4 over time with an effective decay timescale
400 of ~ 3 Ga (e.g. Jaupart et al., 2015) due to the half life of radiogenic elements, there will
401 be a greater effect of mantle plumes during the more recent periods of plate tectonics,
402 including relatively more frequent plume-induced subduction terminations. Such effects
403 due to active upwellings may add to the possible contributions of accumulating damage
404 and persistent sutures in the lithosphere to make plate tectonics more time-dependent
405 toward the present, even though the overall convective vigor may decrease with progres-
406 sive cooling (Foley & Bercovici, 2014; Fuchs & Becker, 2022).

407 As our models are freely convecting, rather than being tailored to specific tectonic
408 scenarios, we can only make observations about what sorts of subduction zones get ter-
409 minated and what the typical geometry and dynamics of those cases are. The main sce-
410 narios we observe are a plume head impinging either in front or behind the subducting
411 slab to cause termination (Figures 2 and 3) and plumes on either side of a subducting
412 slab pinching out a subduction zone leading to termination (Figure 4). The first exam-
413 ple is most common in the model, occurring $\sim 85\%$ of the time in the reference, damage-
414 rheology model, and it is the only mode in the non-damage rheology, lower internal heat-
415 ing, and higher internal heating cases. Typically, this process begins as a plume initi-
416 ating a slab window in the subducting slab. The plume can then either remain station-
417 ary with the subduction zone and the termination happens in the plume's presence, or
418 the plume may advect or diffuse away from the subducting slab, but the influx of heat
419 from the plume was enough to cause the termination. The second scenario has two plumes
420 pinching out a subduction zone to cause a termination. We see this type of termination

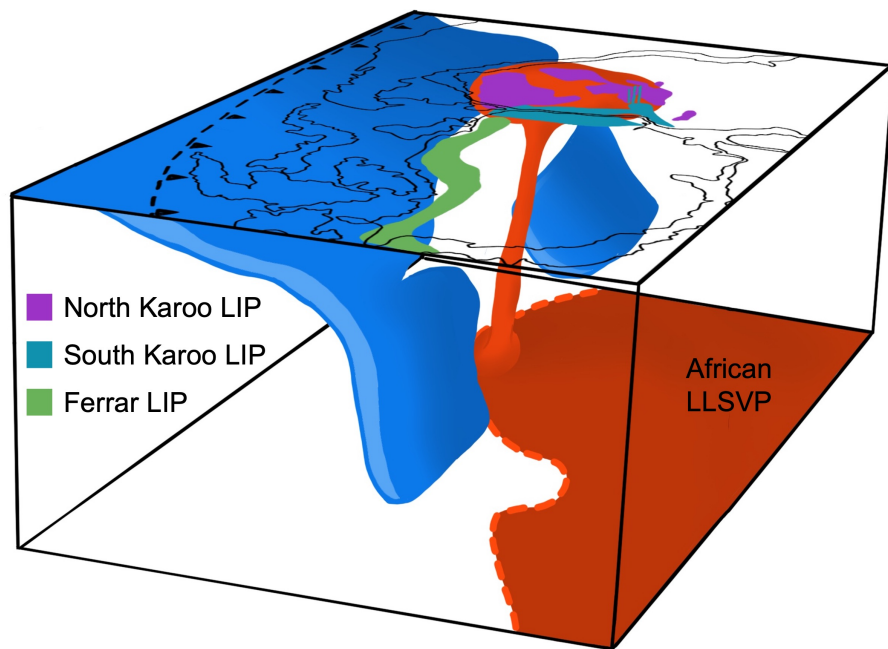
421 less frequently in our models, and this scenario is perhaps also less likely on Earth as it
422 requires plumes on either side of a subduction zone.

423 To discuss disruption frequency of terminations, we must scale back to dimensional
424 Earth time. Thus, we use 300 Myr as an appropriate comparison of overturn time to di-
425 mensional time for Cenozoic mantle convection. The disruption frequency of termina-
426 tions is then one termination every 50 Myr for the lower heating model, every 130 Myr
427 for the reference model, and every 200 Myr for the higher heating model. Additionally,
428 the non-damage model frequency with its one termination would be every 1.8 billion years.
429 This scaling of frequency correlates with the proportion of internal heating of the mod-
430 els, with the most frequent occurring in the model with the highest proportion of bot-
431 tom heating and becoming less frequent with higher proportions of internal heating. This
432 frequency suggests there may be several examples of this plume-slab termination in Earth's
433 history.

434 **4.1 Comparison to past and modern-day tectonic settings**

435 Plume-slab terminations show interesting dynamics in geodynamic models, but there
436 is also some indication of their existence in past and present-day geology. One example
437 during the Jurassic (201-145 Ma) is related to the Karoo-Ferrar LIP eruption in south-
438 western Gondwana. While it is generally agreed that there was a time of flat slab sub-
439 duction previous to the LIP emplacement, there is debate as to how this flat slab sub-
440 duction ended (Dalziel et al., 2000; Luttinen, 2018; Navarrete et al., 2019; Ruhl et al.,
441 2022). Figure 7 shows our interpretation in 3-D of the dynamics of this system, moti-
442 vated by our 3-D model dynamics. If the rising mantle plume was responsible for flat
443 slab subduction (Dalziel et al., 2000), it may have subsequently broke through the slab,
444 reached the lithosphere, and created the Karoo-Ferrar LIP. This scenario can also ex-
445 plain the bilateral geochemical sourcing of the Karoo from both deep mantle sources and
446 subduction-modified upper mantle sources as the plume rises and terminates. The sub-
447 ducting slab could have then unzipped from where the mantle plume broke through, ex-
448 plaining the subduction-influenced upper mantle signature in the Ferrar LIP (Luttinen,
449 2018).

454 A more recent example of plume-slab dynamics is the Arabian-Anatolian-Aegean
455 system (Ershov & Nikishin, 2004; Faccenna et al., 2013; Hua et al., 2023). Subduction

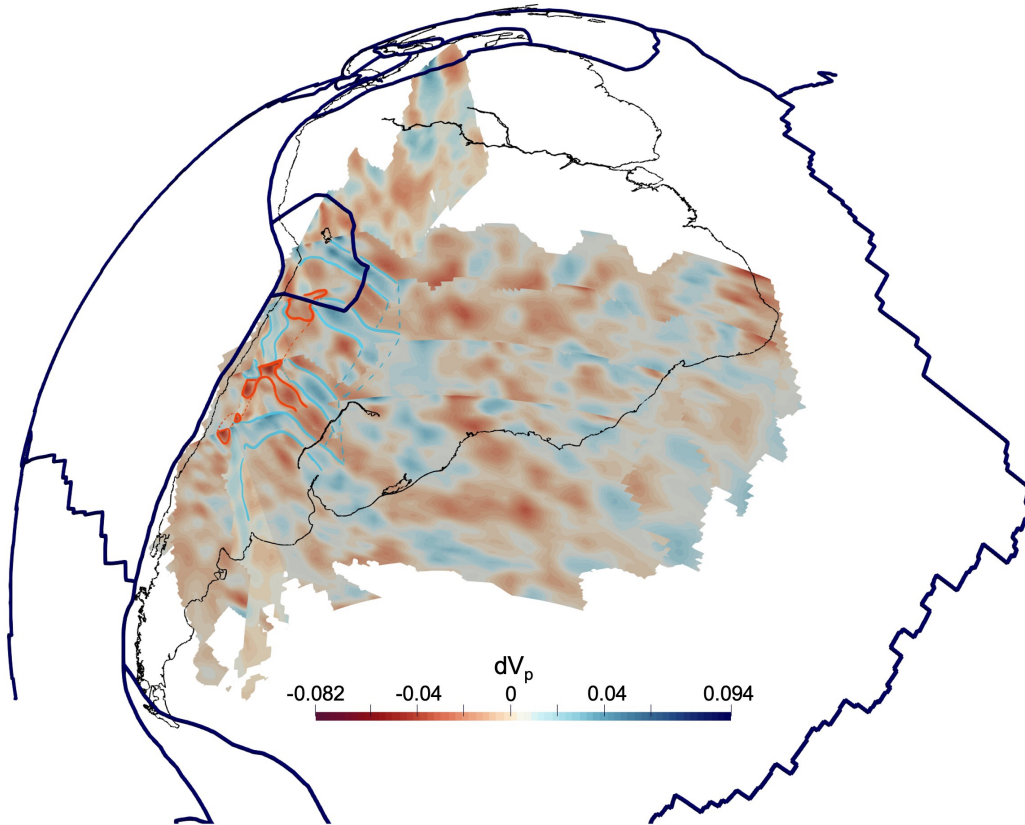


450 **Figure 7.** 3-D reconstruction of southwestern Gondwana during the Jurassic showing on the
451 surface the emplacement of LIPs (Luttinen, 2018). Rendering in the mantle shows projected
452 African LLSVP, mantle plume that cutoff subduction underneath southwestern Gondwana and
453 shows propagation of slab shutoff.

456 in the Mediterranean has been inferred to have been active 30 million years ago as the
457 Afar plume was upwelling under the Arabian plate to the southeast (cf. Faccenna et al.,
458 2013). Volcanic ages and other constraints have been interpreted such that the plume
459 then moved northward toward Anatolia, and that this plume advance was driven or at
460 least assisted by mantle flow, including via a fragmentation of the Mediterranean slab.
461 The formation of a slab gap underneath Anatolia leading to the current Hellenic segment
462 of the trench might have led to asthenospheric suction and contributed to Afar plume
463 advance (Faccenna et al., 2013; Hua et al., 2023). Our results here, and the 2-D mod-
464 els of Heilman and Becker (2022), suggest that the Afar plume may have, in fact, played
465 a more active role in partitioning subduction along the northern margin of Africa.

466 For the modern-day, the Nazca-South American subduction zone may serve as an
467 example for the effect of plumes on slabs. Based on interpretation of seismic tomogra-
468 phy, Portner et al. (2017, 2020) suggested that the Juan de Fuca plume was taking ad-
469 vantage of a previously created slab window. With our model findings, we can specu-
470 late that this interaction is the beginning of a plume-slab termination where a slab win-
471 dow is developed first and a few million years later leads to subduction shutoff. In Fig-
472 ure 8, we interpret the tomography of Portner et al. (2020) for the Nazca slab and man-
473 tle. In this figure the dotted lines are interpretations of the lateral extent of the plume
474 and slab. The mantle plume may have modified and broken through part of the subduct-
475 ing slab. This stage of a plume lying under a subducting slab and creating a slab win-
476 dow is very similar to the beginning stages of several terminations that we observe in
477 our model (i.e. Figure 1). In the future, this interaction may turn into a termination if
478 the slab is sufficiently affected by the presence of the plume.

483 Relevant plume-slab interactions may also be present in other areas for the modern-
484 day, including on the western side of the Pacific where a range of hot anomalies have been
485 imaged in proximity to possibly fragmented slabs (e.g. Obayashi et al., 2009; Tao et al.,
486 2018), and the effects of hot mantle anomalies on subduction have been modeled (e.g.
487 Morishige et al., 2010). Plume-slab interactions in east Asia have been postulated for
488 origin of the Changbaishan volcanic complex, where intraplate volcanism may be driven
489 by a plume disrupting or at least affecting the subducting Pacific plate (Tang et al., 2014).
490 Seismic imaging has been interpreted to show hot material from the deep mantle rising
491 through a gap in the subducting slab (Tang et al., 2014), a type of interaction between
492 plumes and slabs consistent with our model findings.



479 **Figure 8.** Tomography fence diagram of southern South America using dV_p using tomo-
 480 graphic data from Portner et al. (2020). Interpretation of 3D plume-slab interaction structure is
 481 overlain in blue for subducting slab and red for mantle plume. South America is outlined in black
 482 while tectonic plates are outlined in dark blue.

5 Conclusions

We find that plume-induced subduction terminations occurs in 3-D, spherical geometry mantle convection models. Terminations are found throughout our models, but more likely in cases with damage rheology. A single plume can directly shut off subduction by puncturing and cutting off a slab from below, two plumes can pinch out subduction from the side, and a single plume can cause an lateral unzipping of a descending slab. Natural examples where these processes may help explain the thermo-chemical evolution of the continental lithosphere include the Karro-Ferrar LIP, the Afar-Anatolia Agean system, and present-day settings in the western and eastern Pacific subduction systems. Plume-slab termination frequency is inversely related to the proportion of internal heating, implying that plume-slab interactions may have become more prevalent over planetary evolution. Our models can contribute to a better understanding of the relationship between subducting slabs and rising mantle plumes and the effect and expressions of slab-plume “talk-back” in the evolution of the plate tectonic system.

6 Open Research

ASPECT is an open-source mantle convection code hosted by the Computational Infrastructure for Geodynamics, all features used are available in ASPECT version 2.4.0-pre (at aspect.geodynamics.org/), which is available at doi.org/10.5281/zenodo.6903424. The necessary parameter files to replicate models can be found at doi.org/10.5281/zenodo.8102543.

Acknowledgments

This project was funded by the National Science Foundation under award EAR-1853856. We thank the developers and the Computational Infrastructure for Geodynamics (geodynamics.org) which is funded by the National Science Foundation under award EAR-0949446 and EAR-1550901 for supporting the development of ASPECT. We also thank Portner et al. (2020) for making their tomographic model available freely, and J. Dannberg and C. Faccenna for providing comments on a thesis chapter which formed the basis for this manuscript.

521 **References**

- 522 Arnould, M., Coltice, N., Flament, N., & Mallard, C. (2020). Plate tectonics and
 523 mantle controls on plume dynamics. *Earth Planet. Sci. Lett.*, *547*, 116439.
- 524 Auth, C., Bercovici, D., & Christensen, U. R. (2003). Two-dimensional convec-
 525 tion with a self-lubricating, simple-damage rheology. *Geophys. J. Int.*, *154*,
 526 783–800.
- 527 Baes, M., Sobolev, S., Gerya, T., & Brune, S. (2020). Plume-induced subduction
 528 initiation: Single-slab or multi-slab subduction? *Geochem., Geophys., Geosys.*,
 529 *21*(2), e2019GC008663.
- 530 Bercovici, D., & Ricard, Y. (2016). Grain-damage hysteresis and plate tectonic
 531 states. *Phys. Earth Planet. Inter.*, *253*, 31–47.
- 532 Betts, P. G., Mason, W. G., & Moresi, L. (2012). The influence of a mantle plume
 533 head on the dynamics of a retreating subduction zone. *Geology*, *40*(8), 739-
 534 742.
- 535 Dalziel, I. W., Lawver, L., & Murphy, J. (2000). Plumes, orogenesis, and superconti-
 536 nental fragmentation. *Earth and Planetary Science Letters*, *178*(1-2), 1–11.
- 537 Dannberg, J., & Gassmüller, R. (2018). Chemical trends in ocean islands explained
 538 by plume–slab interaction. *Pro. Nat. Acad. Sci.*, *115*, 4351–4356.
- 539 Davies, G. F. (1986). Mantle convection under simulated plates: effects of heating
 540 modes and ridge and trench migration, and implications for the core-mantle
 541 boundary, bathymetry, the geoid and Benioff zones. *Geophys. J. R. Astr. Soc.*,
 542 *84*, 153–183.
- 543 Druken, K., Kincaid, C., Griffiths, R., Stegman, D., & Hart, S. (2014). Plume–slab
 544 interaction: the Samoa–Tonga system. *Phys. Earth Planet. Inter.*, *232*, 1–14.
- 545 Duggen, S., Hoernle, K., Hauff, F., Klügel, A., Bouabdellah, M., & Thirlwall, M. F.
 546 (2009). Flow of Canary mantle plume material through a subcontinental litho-
 547 spheric corridor beneath Africa to the Mediterranean. *Geology*, *37*, 283–286.
- 548 Enns, A., Becker, T. W., & Schmeling, H. (2005). The dynamics of subduction and
 549 trench migration for viscosity stratification. *Geophys. J. Int.*, *160*, 761–775.
- 550 Ershov, A., & Nikishin, A. (2004). Recent geodynamics of the Caucasus-Arabia-east
 551 Africa region. *Geotectonics*, *38*, 123–136.
- 552 Faccenna, C., Becker, T. W., Jolivet, L., & Keskin, M. (2013). Mantle convection in
 553 the Middle East: Reconciling Afar upwelling, Arabia indentation and Aegean

- 554 trench rollback. *Earth Planet. Sci. Lett.*, *375*, 254–269.
- 555 Fletcher, M., & Wyman, D. A. (2015). Mantle plume-subduction zone interactions
556 over the past 60 Ma. *Lithos*, *233*, 162–173.
- 557 Foley, B. J., & Becker, T. W. (2009). Generation of plate tectonics and mantle
558 heterogeneity from a spherical, visco-plastic convection model. *Geochem., Geo-*
559 *phys., Geosys.*, *10*(Q08001). doi: 10.1029/2009GC002378
- 560 Foley, B. J., & Bercovici, D. (2014). Scaling laws for convection with temperature-
561 dependent viscosity and grain-damage. *Geophys. J. Int.*, *199*, 580–603.
- 562 Fraters, M. R. T., Bangerth, W., Thieulot, C., Glerum, A. C., & Spakman, W.
563 (2019). Efficient and practical Newton solvers for nonlinear Stokes systems in
564 geodynamics problems. *Geophys. J. Int.*, *218*, 873–894.
- 565 Fuchs, L., & Becker, T. W. (2019). Role of strain-dependent weakening memory on
566 the style of mantle convection and plate boundary stability. *Geophys. J. Int.*,
567 *218*, 601–618.
- 568 Fuchs, L., & Becker, T. W. (2021). Deformation memory in the lithosphere: A com-
569 parison of damage-dependent weakening and grain-size sensitive rheologies. *J.*
570 *Geophys. Res.*, *126*, e2020JB020335.
- 571 Fuchs, L., & Becker, T. W. (2022). On the role of rheological memory
572 for convection-driven plate reorganizations. *Geophys. Res. Lett.*, *49*,
573 e2022GL099574.
- 574 Gerya, T. V., Bercovici, D., & Becker, T. (2021). Dynamic slab segmentation due to
575 brittle-ductile damage in the outer rise. *Nature*, *599*, 245–250.
- 576 Gerya, T. V., Stern, R. J., Baes, M., Sobolev, S. V., & Whattam, S. A. (2015).
577 Plate tectonics on the Earth triggered by plume-induced subduction initiation.
578 *Nature*, *527*(7577), 221–225.
- 579 Glerum, A., Thieulot, C., Fraters, M., Blom, C., & Spakman, W. (2018). Nonlinear
580 viscoplasticity in ASPECT: benchmarking and applications to subduction.
581 *Solid Earth*, *9*, 267–294.
- 582 Hager, B. H. (1984). Subducted slabs and the geoid: constraints on mantle rheology
583 and flow. *J. Geophys. Res.*, *89*, 6003–6015.
- 584 Heilman, E., & Becker, T. W. (2022). Plume-slab interactions can shut off subduc-
585 tion. *Geophysical Research Letters*, *49*, e2022GL099286.
- 586 Heister, T., Dannberg, J., Gassmüller, R., & Bangerth, W. (2017). High accuracy

- 587 mantle convection simulation through modern numerical methods – II: realistic
588 models and problems. *Geophys. J. Int.*, *210*, 833–851.
- 589 Hua, J., Fischer, K., Gazel, E., Parmentier, E., & Hirth, G. (2023). Long-distance
590 asthenospheric transport of plume-influenced mantle from Afar to Anatolia.
591 *Geochem., Geophys., Geosys.*, *24*, e2022GC010605.
- 592 Jaupart, C., Labrosse, S., Lucazeau, F., & Marechal, J.-C. (2015). Temperatures,
593 heat and energy in the mantle of the Earth. In G. Schubert (Ed.), *Treatise on*
594 *geophysics* (2nd ed., pp. 223–270). Elsevier.
- 595 Kincaid, C., Druken, K., Griffiths, R. W., & Stegman, D. R. (2013). Bifurcation
596 of the Yellowstone plume driven by subduction-induced mantle flow. *Nature*
597 *Geosc.*, *6*, 395–399.
- 598 Koppers, A. A., Becker, T. W., Jackson, M. G., Konrad, K., Müller, R. D., Ro-
599 manowicz, B., ... Whittaker, J. M. (2021). Mantle plumes and their role in
600 earth processes. *Nature Rev. Earth & Environ.*, *2*, 382–401.
- 601 Kronbichler, M., Heister, T., & Bangerth, W. (2012). High accuracy mantle convec-
602 tion simulation through modern numerical methods. *Geophys. J. Int.*, *191*, 12–
603 29.
- 604 Landuyt, W., & Bercovici, D. (2009). Formation and structure of lithospheric shear
605 zones with damage. *Phys. Earth Planet. Inter.*, *175*(115–126).
- 606 Landuyt, W., Bercovici, D., & Ricard, Y. (2008). Plate generation and two-phase
607 damage theory in a model of mantle convection. *Geophys. J. Int.*, *174*, 1065–
608 1080.
- 609 Lavier, L. L., Buck, W. R., & Poliakov, A. N. B. (2000). Factors controlling normal
610 fault offset in an ideal brittle layer. *J. Geophys. Res.*, *105*, 23431–23442.
- 611 Lay, T., Hernlund, J., & Buffett, B. (2008). Core-mantle boundary heat flow. *Nature*
612 *Geosc.*, *1*, 25–32.
- 613 Leng, W., & Zhong, S. (2008). Controls on plume heat flux and plume excess tem-
614 perature. *J. Geophys. Res.*, *113*.
- 615 Liu, L., & Stegman, D. R. (2012). Origin of Columbia River flood basalt controlled
616 by propagating rupture of the Farallon slab. *Nature*, *482*, 386–389.
- 617 Luttinen, A. V. (2018). Bilateral geochemical asymmetry in the Karoo Large Ig-
618 neous Province. *Scientific Reports*, *8*, 5223.
- 619 Mériaux, C., Duarte, J. C., Schellart, W. P., & Mériaux, A.-S. (2015). A two-way

- 620 interaction between the Hainan plume and the Manila subduction zone. *Geo-*
621 *phys. Res. Lett.*, *42*, 5796–5802. doi: 10.1002/2015GL064313
- 622 Moresi, L. N., & Solomatov, V. (1998). Mantle convection with a brittle lithosphere:
623 thoughts on the global tectonic styles of the Earth and Venus. *Geophys. J.*
624 *Int.*, *133*, 669–682.
- 625 Morishige, M., Honda, S., & Yoshida, M. (2010). Possibility of hot anomaly in
626 the sub-slab mantle as an origin of low seismic velocity anomaly under the
627 subducting Pacific plate. *Phys. Earth Planet. Inter.*, *183*, 353–365.
- 628 Navarrete, C., Gianni, G., Encinas, A., Márquez, M., Kamerbeek, Y., Valle, M.,
629 & Folguera, A. (2019). Triassic to Middle Jurassic geodynamic evolution of
630 southwestern Gondwana: From a large flat-slab to mantle plume suction in a
631 rollback subduction setting. *Earth-Science Reviews*, *194*, 125–159.
- 632 Obayashi, M., Yoshimitsu, J., & Fukao, Y. (2009). Tearing of stagnant slab. *Science*,
633 *324*, 1173–1175.
- 634 Obrebski, M., Allen, R. M., Xue, M., & Hung, S.-H. (2010). Slab-plume interaction
635 beneath the Pacific Northwest. *Geophys. Res. Lett.*, *37*(L14305). doi: 10.1029/
636 2010GL043489
- 637 Ogawa, M. (2003). Plate-like regime of a numerically modeled thermal convection in
638 a fluid with temperature-, pressure-, and stress-history-dependent viscosity. *J.*
639 *Geophys. Res.*, *108*(B2), 2067. doi: 10.1029/2000JB000069
- 640 Portner, D. E., Beck, S., Zandt, G., & Scire, A. (2017). The nature of subslab slow
641 velocity anomalies beneath south america. *Geophys. Res. Lett.*, *44*(10), 4747-
642 4755.
- 643 Portner, D. E., Rodríguez, E. E., Beck, S., Zandt, G., Scire, A., Rocha, M. P., . . .
644 others (2020). Detailed structure of the subducted nazca slab into the lower
645 mantle derived from continent-scale teleseismic p wave tomography. *Journal of*
646 *Geophysical Research: Solid Earth*, *125*(5), e2019JB017884.
- 647 Pusok, A. E., & Stegman, D. R. (2020). The convergence history of India-
648 Eurasia records multiple subduction dynamics processes. *Science adv.*, *6*(19),
649 eaaz8681.
- 650 Rey, P. F., Coltice, N., & Flament, N. (2014). Spreading continents kick-started
651 plate tectonics. *Nature*, *513*, 405–408.
- 652 Ricard, Y., Richards, M. A., Lithgow-Bertelloni, C., & Le Stunff, Y. (1993). A geo-

- 653 dynamic model of mantle density heterogeneity. *J. Geophys. Res.*, *98*, 21895–
654 21909.
- 655 Ruhl, M., Hesselbo, S. P., Jenkyns, H. C., Xu, W., Silva, R. L., Matthews, K. J.,
656 ... Riding, J. B. (2022). Reduced plate motion controlled timing of Early
657 Jurassic Karoo-Ferrar large igneous province volcanism. *Science Advances*, *8*,
658 eabo0866.
- 659 Stein, C., & Hansen, U. (2013). Arrhenius rheology versus Frank-Kamenetskii
660 rheology—Implications for mantle dynamics. *Geochem., Geophys., Geosys.*, *14*,
661 2757–2770. doi: 10.1002/ggge.20158
- 662 Steinberger, B., & Calderwood, A. (2006). Models of large-scale viscous flow in the
663 Earth’s mantle with constraints from mineral physics and surface observations.
664 *Geophys. J. Int.*, *167*, 1461–1481.
- 665 Sun, D., Miller, M. S., Holt, A. F., & Becker, T. W. (2014). Hot upwelling conduit
666 beneath the Atlas Mountains, Morocco. *Geophys. Res. Lett.*, *41*, 8037–8044.
667 doi: 10.1002/2014GL061884
- 668 Tackley, P. J. (2000a). Self-consistent generation of tectonic plates in time-
669 dependent, three-dimensional mantle convection simulations 1. Pseudoplastic
670 yielding. *Geochem., Geophys., Geosys.*, *1*(1021). doi: 10.1029/2000GC000036
- 671 Tackley, P. J. (2000b). Self-consistent generation of tectonic plates in time-
672 dependent, three-dimensional mantle convection simulations 2. Strain weak-
673 ening and asthenosphere. *Geochem., Geophys., Geosys.*, *1*(1026). doi:
674 10.1029/2000GC000043
- 675 Tan, E., Gurnis, M., & Han, L. (2002). Slabs in the lower mantle and their modula-
676 tion of plume formation. *Geochem., Geophys., Geosys.*, *3*(1067). doi: 10.1029/
677 2001GC000238
- 678 Tang, Y., Obayashi, M., Niu, F., Grand, S. P., Chen, Y. J., Kawakatsu, H., ...
679 Ni, J. F. (2014). Changbaishan volcanism in northeast China linked to
680 subduction-induced mantle upwelling. *Nature Geoscience*, *7*, 470–475.
- 681 Tao, K., Grand, S. P., & Niu, F. (2018). Seismic structure of the upper mantle
682 beneath Eastern Asia from full waveform seismic tomography. *Geochem., Geo-
683 phys., Geosys.*, *19*, 2732–2763.
- 684 Ueda, K., Gerya, T., & Sobolev, S. V. (2008). Subduction initiation by thermal-
685 chemical plumes: numerical studies. *Phys. Earth Planet. Inter.*, *171*, 296–312.

- 686 van Heck, H., & Tackley, P. J. (2008). Planforms of self-consistently generated plate
 687 tectonics in 3-D spherical geometry. *Geophys. Res. Lett.*, *35*(L19312). doi: 10
 688 .1029/2008GL035190
- 689 van Hinsbergen, D. J. J., Steinberger, B., Doubrovine, P., & Gassmüller, R. (2011).
 690 Acceleration-deceleration cycles of India-Asia convergence: roles of man-
 691 tle plumes and continental collision. *J. Geophys. Res.*, *116*(B06101). doi:
 692 10.1029/2010JB008051
- 693 van Hinsbergen, D. J. J., Steinberger, B., Guilmette, C., Maffione, M., Gürer, D.,
 694 Peters, K., ... others (2021). A record of plume-induced plate rotation trigger-
 695 ing subduction initiation. , *14*, 626–630.
- 696 van Hunen, J., & van den Berg, A. P. (2008). Plate tectonics on the early Earth:
 697 limitations imposed by strength and buoyancy of subducted lithosphere.
 698 *Lithos*, *103*, 217-235.
- 699 Zhong, S. (2006). Constraints on thermochemical convection of the mantle from
 700 plume heat flux, plume excess temperature and upper mantle temperature. *J.*
 701 *Geophys. Res.*, *111*. doi: 10.1029/2005JB003972